

## RESEARCH ARTICLE

10.1002/2018JC013787

## Key Points:

- Multiple formulations of export efficiency were applied to satellite-based data to estimate carbon export in the Southern Ocean
- Novel lidar and MODIS data were combined to estimate phytoplankton biomass and primary productivity throughout the full annual cycle
- The best export efficiency model is based on a negative productivity versus e-ratio relationship, and accounts for Si-induced ballasting

## Supporting Information:

- Supporting Information S1
- Figure S1
- Figure S2

## Correspondence to:

L. Arteaga,  
laaq@princeton.edu

## Citation:

Arteaga, L., Haëntjens, N., Boss, E., Johnson, K. S., & Sarmiento, J. L. (2018). Assessment of export efficiency equations in the southern ocean applied to satellite-based net primary production. *Journal of Geophysical Research: Oceans*, 123, 2945–2964. <https://doi.org/10.1002/2018JC013787>


Received 12 JAN 2018

Accepted 27 MAR 2018

Accepted article online 6 APR 2018

Published online 26 APR 2018

## Assessment of Export Efficiency Equations in the Southern Ocean Applied to Satellite-Based Net Primary Production

Lionel Arteaga<sup>1</sup> , Nils Haëntjens<sup>2</sup> , Emmanuel Boss<sup>2</sup> , Kenneth S. Johnson<sup>3</sup> , and Jorge L. Sarmiento<sup>1</sup> 

<sup>1</sup>Program in Atmospheric and Oceanic Sciences, Princeton University, 300 Forrester Rd, Princeton, NJ, USA, <sup>2</sup>School of Marine Sciences, University of Maine, Orono, ME, USA, <sup>3</sup>Monterey Bay Aquarium Research Institute, Moss Landing, CA, USA

**Abstract** Carbon export efficiency (e-ratio) is defined as the fraction of organic carbon fixed through net primary production (NPP) that is exported out of the surface productive layer of the ocean. Recent observations for the Southern Ocean suggest a negative e-ratio versus NPP relationship, and a reduced dependency of export efficiency on temperature, different than in the global domain. In this study, we complement information from a passive satellite sensor with novel space-based lidar observations of ocean particulate backscattering to infer NPP over the entire annual cycle, and estimate Southern Ocean export rates from five different empirical models of export efficiency. Inferred Southern Ocean NPP falls within the range of previous studies, with a mean estimate of 15.8 ( $\pm$  3.9) Pg C yr<sup>-1</sup> for the region south of 30°S during the 2005–2016 period. We find that an export efficiency model that accounts for silica(Si)-ballasting, which is constrained by observations with a negative e-ratio versus NPP relationship, shows the best agreement with in situ-based estimates of annual net community production (annual export of 2.7  $\pm$  0.6 Pg C yr<sup>-1</sup> south of 30°S). By contrast, models based on the analysis of global observations with a positive e-ratio versus NPP relationship predict annually integrated export rates that are  $\sim$  33% higher than the Si-dependent model. Our results suggest that accounting for Si-induced ballasting is important for the estimation of carbon export in the Southern Ocean.

**Plain Language Summary** The amount of organic carbon that is exported from the surface to the deep ocean exerts an important control on atmospheric carbon dioxide and the transfer of organic material across trophic levels. In this study, we make use of novel satellite information, combined with autonomous profiling floats, to estimate the efficiency and the amount of organic carbon exported in the Southern Ocean by phytoplankton. We find that previous global formulations can overestimate the amount of carbon exported in this region, and that taking into account the oceanic surface silica concentration is necessary to accurately estimate carbon export in the Southern Ocean.

## 1. Introduction

The export of organic carbon produced by photosynthetic organisms from the surface euphotic layer to the deep ocean exerts an important control over the global distribution of nutrient chemical elements, marine food webs, and the Earth's climate through the regulation of atmospheric CO<sub>2</sub> (Sarmiento & Bender, 1994; Volk & Hoffert, 1985). The vertical export of carbon and associated biogeochemically relevant elements in the Southern Ocean is of major significance as it constrains the horizontal export of nutrients from this region toward lower latitudes, which drives up to 75% of the biological production north of 30°S (Sarmiento et al., 2004a). Changes in the efficiency of nutrient utilization in the Southern Ocean have the potential to alter not only the atmospheric CO<sub>2</sub> concentration, but also the distribution of low-latitude primary production (Sarmiento & Orr, 1991; Sarmiento et al., 2004a).

Carbon export efficiency (e-ratio) is defined as the fraction of organic carbon fixed through net primary production (NPP) that is exported out of the surface productive layer of the ocean. Global observations of marine productivity and particle export generally show a positive relationship between carbon export efficiency and NPP, and a negative (or inverse) relationship between export efficiency and temperature (Dunne

et al., 2005; Eppley & Peterson, 1979; Henson et al., 2011; Laws et al., 2000; Laws et al., 2011). As a result, several empirical models have been developed relating the e-ratio, and derived carbon export rates, to satellite-based information of NPP, and sea surface temperature (SST) (Henson et al., 2011; Laws et al., 2011). However, recent evidence suggests that the relationship between e-ratio, NPP, and temperature may be different in certain oceanic regions, particularly, in the Southern Ocean, suggesting that global parameterizations of export efficiency may show important biases in this region (Le Moigne et al., 2016; Maiti et al., 2013). A compilation of directly measured primary production rates and particle export estimates derived from drifting sediment traps and thorium-234 ( $^{234}\text{Th}$ ) based measurements (Maiti et al., 2013) shows an inverse relationship between primary productivity and export efficiency, and a weak relationship between temperature and export efficiency for the oceanic region south of  $40^{\circ}\text{S}$ . Several studies have investigated the possible causes for this relationship, suggesting that bacteria and zooplankton may play an important role in the regulation of export efficiency through grazing, remineralization of organic matter, and production/export of fecal pellets (Cavan et al., 2015, 2017; Laurenceau-Cornec et al., 2015; Le Moigne et al., 2016). Recently, Britten et al. (2017) suggested that the silica-induced ballasting effect of particles obscures the relationship between export efficiency and temperature in the Southern Ocean, and that accounting for this ballasting effect reveals the expected inverse effect of temperature on export efficiency. While these efforts begin to provide insight into the mechanisms regulating carbon export efficiency in the Southern Ocean, the quantitative implications of these contrasting relationships (between e-ratio, NPP, and temperature) for the estimation of carbon export have not yet been addressed.

Light detection and ranging (lidar) systems have the potential to retrieve optical information under conditions where passive sensors are unable to operate (e.g., during night time, thin clouds, and low solar angles). Lidar systems have been used on board ships and aircrafts to estimate marine optical properties and ecosystem variables (e.g., phytoplankton pigments, zooplankton biomass, sardines density) (Churnside & Thorne, 2005; Churnside et al., 1997; Dickey et al., 2011; Hoge et al., 1988). The applications of lidar instruments are particularly relevant for polar regions such as the Southern Ocean, where biogeochemical fluxes are difficult to quantify due to harsh environmental conditions preventing the continuity of in situ ship surveys, and the inability of passive satellite ocean colour sensors to retrieve information during dark (winter) months. The first application of lidar observations from space to quantify marine biogeochemical properties is that of Behrenfeld et al. (2013), which aimed to estimate phytoplankton carbon and particulate organic carbon (POC) from ocean particulate backscattering ( $b_{bp}$ ) data obtained by the Cloud-Aerosol Lidar with Orthogonal Polarization (CALIOP) sensor (Hunt et al., 2009; Winker et al., 2009). More recently, Behrenfeld et al. (2017) were able to infer polar phytoplankton blooms from lidar-based  $b_{bp}$  observations, improving the reach of polar satellite biogeochemical observations commonly achieved by passive satellite sensors (e.g., the Sea-Viewing Wide Field-of-View Sensor (SeaWiFS), or the Moderate Resolution Imaging Spectroradiometer (MODIS)).

In the present study, we further exploit the space-based lidar data set by complementing missing information from MODIS chlorophyll (Chl) retrievals with Chl estimates derived from CALIOP phytoplankton carbon biomass ( $C_{\text{phyto}}$ ). We use this merged MODIS and CALIOP Chl product ( $\text{Chl}_{\text{merged}}$ ), combined with CALIOP  $C_{\text{phyto}}$ , to quantify net primary production rates through the full annual cycle in the Southern Ocean over the entire period of available lidar  $b_{bp}$  data (June 2006 to August 2015). Monthly composites of NPP are used to obtain estimates of carbon export derived from five simple empirical models (equations) of export efficiency, with different e-ratio, NPP, and temperature relationships. Inferred rates of annual carbon export are compared with a compilation of in situ-based estimates of annual net community production (ANCP) (considered equivalent to export production under steady-state conditions; Ducklow & Doney, 2013) largely derived from profiling floats observations as part of the Southern Ocean Carbon and Climate Modeling and Observations (SOCCOM) program. Ultimately, we provide a quantitative assessment of the implications of different relationships between export efficiency, primary productivity, and temperature on carbon export rates in the Southern Ocean.

## 2. Methods

### 2.1. Estimates of Net Primary Production

Following Dunne et al. (2007) and Sarmiento et al. (2004b), we estimate primary productivity from satellite information on surface Chl, SST, and photosynthetically active radiation (PAR) using the Vertically

Generalized Production Model (VGPM; Behrenfeld & Falkowski, 1997), the model by Carr (2002) (hereinafter Carr02), and the model by Lee et al. (1996) as implemented by Marra et al. (2003) (hereinafter Marra03). The most important difference between these models lies in the sensitivity of their photosynthetic rate to temperature. The VGPM shows an increase in modeled NPP with increasing temperature, reaching a maximum at 20°C, followed by a decrease in NPP at higher temperatures (>20°C). This reduction in productivity is related to the connection between warmer waters and increased nutrient limitation in the ocean (Behrenfeld & Falkowski, 1997). The Carr02 and Marra03 models show a more continuous increase in NPP with temperature (Sarmiento et al., 2004b). A comprehensive assessment of the uncertainty associated to NPP models is presented in Friedrichs et al. (2009), Carr et al. (2006), and Campbell et al. (2002).

We include a fourth model, a Carbon-based Productivity Model (CbPM05; Behrenfeld et al., 2005), which is based on phytoplankton carbon as indicator of phytoplankton biomass, rather than chlorophyll. We employ the earlier version of this model (Behrenfeld et al., 2005) as it is constrained by the same satellite information as the other three productivity models described above, with the exception of the light attenuation coefficient at 490 nm ( $K_{490} \text{ m}^{-1}$ ).  $K_{490}$  is estimated from an empirical relationship with Chl derived by Morel et al. (2007):

$$K_{490} = 0.166 + 0.0773 \times \text{Chl}(\text{mg m}^{-3})^{0.06715} \quad (1)$$

The satellite information on SST (°C), and PAR ( $\text{mol quanta m}^{-2}$ ), used as input for these models was obtained as monthly Level 3 MODIS products from <http://www.science.oregonstate.edu/ocean.productivity/site.php> for the period 2006–2015, and regridded to a 1° by 1° resolution. The estimation of satellite phytoplankton biomass (Chl and Cphyto) is detailed below.

## 2.2. Phytoplankton Carbon and Chlorophyll

Information on surface Chl concentration from MODIS ( $\text{Chl}_{\text{MODIS}}$ ) for the same period is obtained as monthly Level 3 MODIS products from <http://www.science.oregonstate.edu/ocean.productivity/site.php>. Regions of missing  $\text{Chl}_{\text{MODIS}}$  data are filled with lidar-based Chl ( $\text{Chl}_{\text{CALIOP}}$ ) estimates inferred from CALIOP Cphyto ( $\text{mg C m}^{-3}$ ). In order to estimate Cphyto, we make use of all available (day and night)  $b_{bp}$  at 440 nm data from CALIOP obtained as monthly mean files for June 2006 to August 2015 from <http://orca.science.oregonstate.edu/lidar.php>, regridded to a 1° by 1° resolution grid following Behrenfeld et al. (2017). Regions of no data (gaps) in mean monthly CALIOP  $b_{bp}$  maps are filled by performing a 2D interpolation based on the construction of partial differential equations constrained by the boundary values surrounding the gaps (function inpaint\_nans.m, <https://www.mathworks.com/matlabcentral/fileexchange/4551-inpaint-nans>). Phytoplankton carbon biomass is obtained using an empirically derived relationship between Cphyto and  $b_{bp}$  (Behrenfeld et al., 2005, 2017; Graff et al., 2015):

$$\text{Cphyto} = 12128 \text{ mg C m}^{-2} \times (b_{bp} - 0.00035 \text{ m}^{-1}). \quad (2)$$

$\text{Chl}_{\text{CALIOP}}$  is computed as the product of Cphyto and a Chl:C ratio of 0.01 ( $\text{gr gr}^{-1}$ ). A Chl:C ratio of 0.01 ( $\text{gr gr}^{-1}$ ) was determined from an evaluation of the four productivity models under different Chl:C ratios used to estimate  $\text{Chl}_{\text{CALIOP}}$  (see next section).  $\text{Chl}_{\text{CALIOP}}$  complements our  $\text{Chl}_{\text{MODIS}}$  maps in regions of missing MODIS retrievals. We refer to this final merged ( $\text{Chl}_{\text{MODIS}}$  and  $\text{Chl}_{\text{CALIOP}}$ ) product as  $\text{Chl}_{\text{merged}}$ .

NPP estimates from the VGPM, Marra03, and Carr02 models used  $\text{Chl}_{\text{merged}}$  as their phytoplankton biomass input. The CbPM05 estimates NPP using Cphyto as its indicator of phytoplankton biomass. Since our goal is to compute NPP and carbon export rates, we mask out pixels where the satellite PAR product is not computed (given that PAR is essential for calculations of primary productivity). This includes conditions where Top-of-Atmosphere (TOA) radiance is negative, high solar glint, and/or sea ice. We apply this mask to our satellite-based Cphyto, and derived Chl, NPP, e-ratio, and carbon export estimates.

## 2.3. Determination of Chl:C for Lidar-Based Chlorophyll

A priori, it is not clear what the correct magnitude of the Chl:C ratio is in regions where optical data from MODIS is missing: On one hand, low light levels during winter should result in light limitation of phytoplankton growth, inducing high Chl:C ratios as a photoacclimation response (Arteaga et al., 2016; Geider, 1987; MacIntyre et al., 2000); On the other hand, well known iron limiting conditions in the Southern Ocean (Boyd et al., 2007; Martin, 1990) should reduce Chl synthesis and decrease the Chl:C ratio (Geider & LaRoche, 1994; Sunda

& Huntsman, 1997). In order to determine the Chl:C ratio that results in satellite estimates of NPP that are most consistent with existing in situ observations of NPP, we carried out 28 simulations of NPP for each productivity model (i.e., 112 simulations in total), varying the Chl:C ratio across three orders of magnitude, from 0.1 to 0.0001 g Chl g<sup>-1</sup>, in those regions where Chl<sub>MODIS</sub> information is missing, and Chl<sub>CALIOP</sub> is estimated instead (supporting information Figure S1). Satellite NPP estimates are grouped into a monthly climatology representative of a mean annual cycle between 2006 and 2015. We compare the resulting satellite NPP climatology with a data base of in situ carbon-14 (<sup>14</sup>C) based productivity measurements for the Southern Ocean (Buitenhuis et al., 2013). The in situ observations were provided as vertically integrated NPP (E. Buitenhuis, personal communication, 2017) containing 205 data points for the region south of 30°S, were daily measurements of <sup>14</sup>C-NPP are grouped by month. All four models show a significant reduction in the root-mean-square error (RMSE) between predicted and observed NPP around 0.01 g Chl g<sup>-1</sup> C, despite a small reduction in the coefficient of determination (R<sup>2</sup>, obtained from a type II regression model; York, 1966) (supporting information Figure S1). A Chl:C = 0.01 g g<sup>-1</sup> was chosen to compute Chl<sub>CALIOP</sub> from C<sub>phyto</sub> as this value provides the largest relative improvement in the comparison between in situ and modeled NPP rates (largest reduction in RMSE). For simplicity, we assume no seasonality in Chl:C, which is consistent with small Chl:C seasonal variability estimated from optical methods in the Sub-Antarctic Zone (Thomalla et al., 2017). We do not use this data comparison exercise to define the best NPP model, but instead use all four models to develop a range of uncertainty between estimates. Monthly 1° by 1° NPP maps between June 2006 and August 2015, are obtained from each of these models, based on inferred Chl<sub>merged</sub> and C<sub>phyto</sub> in the Southern Ocean.

#### 2.4. Equations of Export Efficiency

We assess patterns in Southern Ocean export efficiency (e-ratio) derived from five different simple empirical models of the e-ratio. Two of these models, which are derived from the analysis of global observations of NPP and carbon export, represent a positive relationship between e-ratio and NPP (or biomass) (Dunne et al., 2005; Laws et al., 2011):

$$\text{e-ratio} = -0.0081 \times T + 0.0668 \times \ln(\text{Chl}_{\text{int}}/Z_{\text{eu}}) + 0.426 \quad (\text{equation Dunne05})$$

$$\text{e-ratio} = 0.04756 \times \left(0.78 - \frac{0.43T}{30}\right) \text{NPP}^{0.307} \quad (\text{equation Laws11})$$

where T is temperature (°C) (input as SST), NPP is in mg C m<sup>-2</sup> d<sup>-1</sup>, Z<sub>eu</sub> is the euphotic depth (m) (depth with 1% of PAR), and Chl<sub>int</sub> is vertically integrated chlorophyll from surface to Z<sub>eu</sub> (mg Chl m<sup>-2</sup>). The third

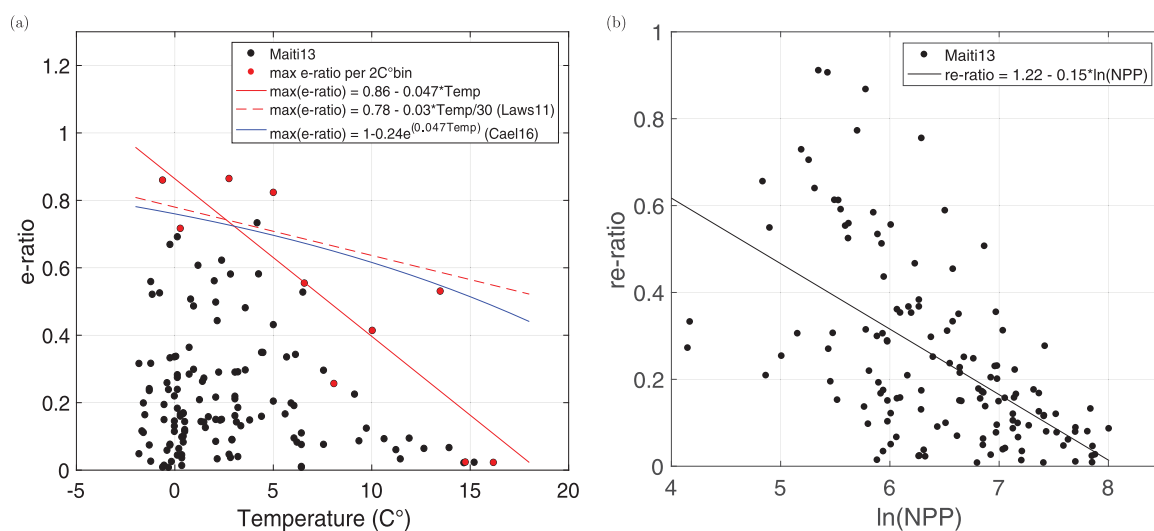


**Figure 1.** (a) Relationship between e-ratio and temperature in the data set compiled by Maiti et al. (2013). The highest e-ratios at each 2°C interval (red dots) are used to constrain a linear regression between the maximum e-ratio (max(e-ratio)) and temperature (solid red line). The empirical and mechanistic temperature dependence of the max(e-ratio) derived by Laws et al. (2011) (dashed red line), and Cael and Follows (2016) (solid blue line), respectively, are also shown. (b) Relationship between normalized e-ratio (re-ratio) and ln(NPP) (NPP units are mg C m<sup>-2</sup> d<sup>-1</sup>) for the same data set. Solid black line is the linear regression model between the variables.

empirical model does not use NPP as a predictor variable, and relies on temperature alone to infer the e-ratio (Henson et al., 2011):

$$\text{e-ratio} = 0.23 \exp^{(-0.08T)} \quad (\text{equation Henson11})$$

The fourth empirical model is derived from a data set of matching NPP and particle export estimates for the Southern Ocean (south of 40°S; Maiti et al., 2013), and includes silicate surface concentration, [Si], as a predictor of the e-ratio (Britten et al., 2017)

$$\text{e-ratio} = (b_1 + b_2T + b_4[\text{Si}])\text{NPP}^{b_3} \quad (\text{equation Britten17})$$

where coefficients  $b_1 = 3.72$ ,  $b_2 = -0.16$ ,  $b_3 = -0.55$  and  $b_4 = -0.04$  are obtained from Table 1 in Britten et al. (2017) (corresponding to the Si model for all observations, drifting sediment traps and <sup>234</sup>Th-based, compiled in Maiti et al., 2013). NPP in equation Britten17 is in units of  $\text{mmol C m}^{-2} \text{d}^{-1}$ . Surface ocean [Si] ( $\text{mmol m}^{-3}$ ), is obtained from the World Ocean Atlas 2013 monthly climatology (Garcia et al., 2014), (available at <http://www.nodc.noaa.gov/OC5/woa13/>) (equation Britten17 has been corrected with respect to its original publication after personal communication with the authors clarified that subtraction signs should be substituted for addition signs in Britten et al. (2017).

Finally we derive a fifth empirical model following a set of similar steps as in Laws et al. (2011) to constrain the e-ratio as a function of temperature and NPP ( $\text{mg C m}^{-2} \text{d}^{-1}$ ), using the Southern Ocean data set of Maiti et al. (2013). First, we constrain the maximum e-ratio as a function of temperature by fitting a least square linear regression model through the maximum e-ratio ( $\text{max}(\text{e-ratio})$ ) in each temperature interval separated by 2°C (from -2 to 18 °C) (red symbols in Figure 1a). The slope of this relationship between  $\text{max}(\text{e-ratio})$  and temperature is larger (i.e., more negative) than the empirical relation set in Laws et al. (2011), and that of Cael and Follows (2016), which is based on the difference in the temperature sensitivity of autotrophic and heterotrophic metabolic rates. Subsequently, we normalize all e-ratios by the maximum e-ratio predicted by the regression in Figure 1a, and fit a least square linear regression model between the normalized e-ratios ( $\text{re-ratio} = \frac{\text{e-ratio}}{\text{max}(\text{e-ratio})}$ ) and log-transformed NPP (Figure 1b). Combined with the dependence of  $\text{max}(\text{e-ratio})$  on temperature, the final empirical equation for the estimation of export efficiency in the Southern Ocean has the following form ( $\pm$  standard error):

$$\text{e-ratio} = (0.86 (\pm 0.09) - 0.047 (\pm 0.01) \text{Temp}) \times (1.22 (\pm 0.12) - 0.15 (\pm 0.018) \log(\text{NPP})) \quad (\text{equation SO})$$

Equation Britten17 and equation SO are both based on the negative relationship between export efficiency and primary productivity observed in the Southern Ocean (Maiti et al., 2013). However, equation SO does not account for the ballasting effect of Si. We force these five empirical models, constrained by different data sets with distinct inherent relationships between export efficiency, primary productivity, and temperature, with satellite-based Chl, NPP, SST, and surface Si WOA13 climatology to obtain estimates of the e-ratio. By combining our inferred NPP and e-ratio estimates derived from these empirical models, we are able to quantify the implications of different relationships between the e-ratio, NPP, and temperature for derived estimates of organic carbon export in the Southern Ocean. Our satellite-based Chl, NPP, e-ratio, and carbon export data set is composed of monthly Southern Ocean 1° by 1° maps between June 2006 and August 2015.

**Table 1**  
Mean Zonally Integrated NPP for the Oceanic Area South of 50° for the Period 2006–2015

This study	Pg C yr <sup>-1</sup>	Previous studies	Pg C yr <sup>-1</sup>
VGPM	3.0	Arrigo et al. (1998)	4.4
Marra03	3.4	Moore and Abbott (2000)	2.9
Carr02	2.7	Arrigo et al. (2008)	1.9
CbPM05	1.8	Shang et al. (2010) (CbPM08) <sup>a</sup>	1.7
Mean	2.7 ± 0.6 <sup>b</sup>	Shang et al. (2010) (VGPM)	1.3

<sup>a</sup>Refers to the updated CbPM (Westberry et al., 2008). <sup>b</sup>Standard deviation of NPP models.

### 3. Results and Discussion

#### 3.1. Inferred Chlorophyll

The largest gain in photosynthetic biomass information from CALIOP is evident in the  $\text{Chl}_{\text{merged}}$  product during austral winter (May–July), where missing retrievals in  $\text{Chl}_{\text{MODIS}}$  extend southward of ~ 40°S (Figures 2a and 2b). As described above, estimates of  $\text{Chl}_{\text{CALIOP}}$  are obtained as the product of CALIOP-based  $C_{\text{phyto}}$  and a Chl:C ratio of 0.01 ( $\text{g g}^{-1}$ ) assigned to regions with no Chl estimates in  $\text{Chl}_{\text{MODIS}}$ . In regions with available  $\text{Chl}_{\text{MODIS}}$  data, the Chl:C ratio is defined as the ratio of Chl from MODIS and phytoplankton carbon from CALIOP ( $\text{Chl}_{\text{MODIS}} : C_{\text{phyto}}$ ) (Figure 2c). A Chl:C = 0.01 ( $\text{g g}^{-1}$ ) is a realistic ratio

expressed in nutrient-limited phytoplankton cells, observed in both the field and laboratory cultures (Arteaga et al., 2016; Behrenfeld et al., 2005; Pahlow et al., 2013). Interestingly,  $0.01 \text{ g Chl g C}^{-1}$  was found to be the median ratio in laboratory data compiled by Behrenfeld et al. (2002) for light levels between 0.7 and  $1.4 \text{ moles photons m}^{-2} \text{ h}^{-1}$ . Haëntjens et al. (2017) computed Chl:C ratios for an extensive array of floats equipped with bio-optical sensors deployed in the Southern Ocean and found the highest frequency of Chl:C to be centered around  $0.01 \text{ g Chl g C}^{-1}$ . The normalized frequency histogram of  $\text{Chl}_{\text{merged}}$  does not deviate significantly from the frequency distribution of  $\text{Chl}_{\text{MODIS}}$  (Figure 2d), and also matches the frequency distribution of (passive) satellite (MODIS and Visible Infrared Imaging Radiometer Suite (VIIRS)) and float matchups observed in the Southern Ocean (Haëntjens et al., 2017). These observations suggest that  $0.01 \text{ g Chl g C}^{-1}$  is a reasonable value to assign in regions of the Southern Ocean where the actual Chl:C ratio is unknown.

A Chl:C ratio of 0.01 ( $\text{g g}^{-1}$ ) also coincides with the Chl:C ratio predicted in oligotrophic, nutrient limited areas of the Atlantic and Pacific oceans (Arteaga et al., 2016; Behrenfeld et al., 2005, 2016). A relatively low Chl:C ratio in the Southern Ocean suggests a “break down” of the photoacclimation mechanism of the cells, which should otherwise induce chlorophyll synthesis (and consequently high Chl:C) as a response to low light levels in this high latitude/deep mixing area (Dong et al., 2008). This “break down” might be caused by

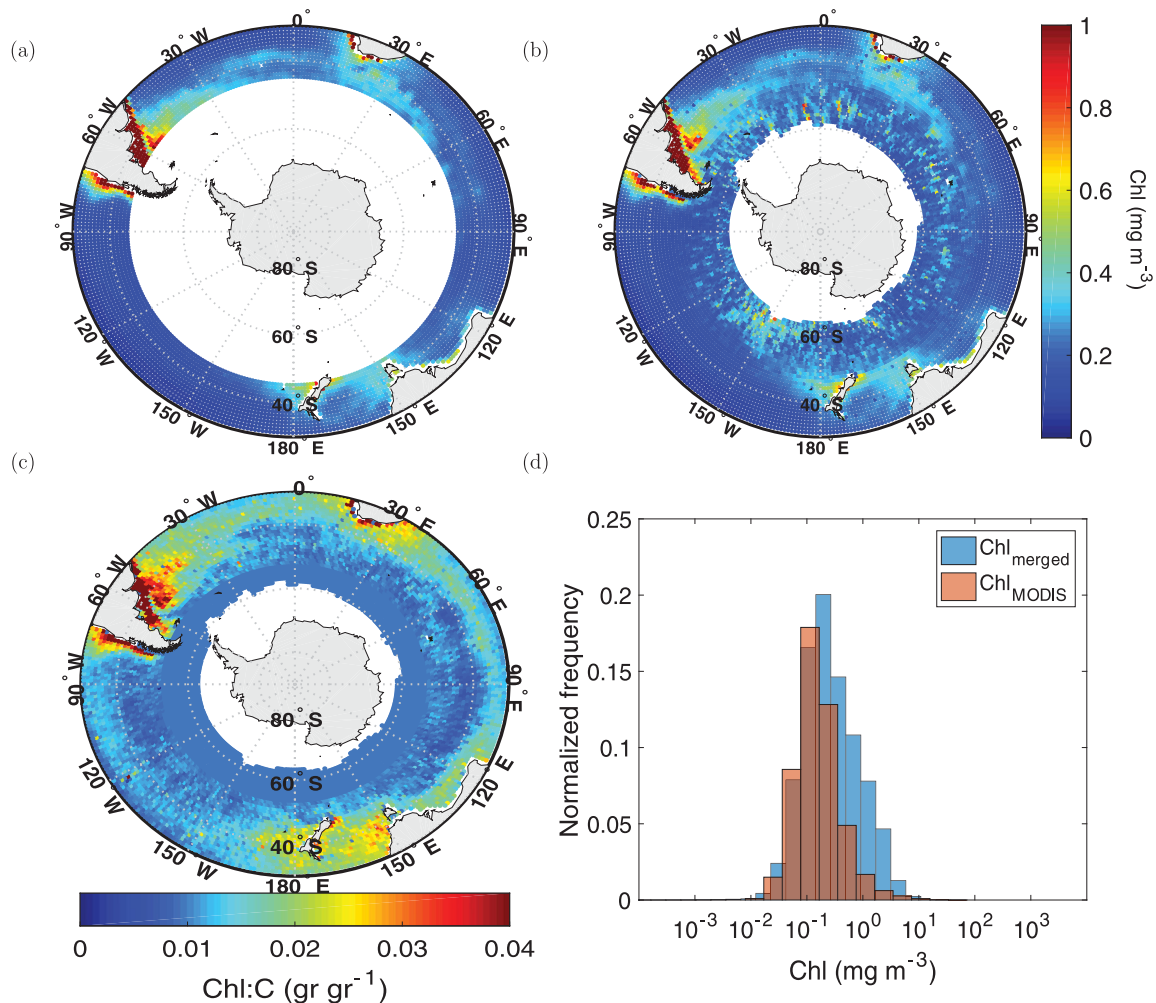


**Figure 2.** Climatology of mean surface chlorophyll concentration ( $\text{mg Chl m}^{-3}$ ) estimated by (a) MODIS ( $\text{Chl}_{\text{MODIS}}$ ), and (b) CALIOP and MODIS merged product ( $\text{Chl}_{\text{merged}}$ ) for austral winter months (mean of May–July) in the Southern Ocean (period June 2006 to August 2015). Estimates of surface Chl from CALIOP in  $\text{Chl}_{\text{merged}}$  are obtained by assigning a Chl:C ratio of  $0.01 \text{ (g g}^{-1}\text{)}$  to regions with no information in  $\text{Chl}_{\text{MODIS}}$ . (c) Chl:C ratio ( $\text{gr gr}^{-1}$ ) ( $\text{Chl}_{\text{MODIS}}$ : Cphyto) during winter in the Southern Ocean. (d) Normalized frequency histogram of chlorophyll concentration obtained from  $\text{Chl}_{\text{MODIS}}$  and  $\text{Chl}_{\text{merged}}$ . White areas are regions of missing Chl retrievals.

a decrease in the electron transfer efficiency of the photosynthetic apparatus due to iron limitation (Geider & LaRoche, 1994), and/or a chemical reduction of the plastoquinone pool (PQ), which downregulates chlorophyll synthesis under extreme light limiting conditions (Behrenfeld et al., 2016).

### 3.2. Southern Ocean NPP

All four productivity models used in this study show a similar spatial pattern of inferred NPP in the Southern Ocean (Figure 3). The VGPM shows the highest NPP estimates along the high productivity region between the 40°S and 60°S in all three basins (Atlantic, Indian, and Pacific) of the Southern Ocean (Figures 3a and 3b). The Marra03 model shows overall lower meridional variability in predicted NPP (Figures 3c and 3d). These two models yield higher NPP rates than the Carr02 and CbPM05 models (Figures 3e–3f, and 3g–h, respectively). All four models show similar seasonal (winter and summer) patterns. We use the mean product from these models as our main satellite-based NPP product for the Southern Ocean (Figures 3i and 3j).

We evaluate NPP estimates in four distinct environmental regions of the Southern Ocean (defined as the oceanic region south of 30°S): The Sub-tropical Zone (STZ), Sub-Antarctic Zone (SAZ), Polar-Antarctic Zone (PAZ), and Seasonal-ice Zone (SIZ) (Figure 4a). These environmental regions are defined based on a mean 2004–2014 Argo-based climatology of temperature and salinity (Roemmich & Gilson, 2009), following the criteria of Orsi et al. (1995), and computed by Bushinsky et al. (2017). The SAZ and STZ are the most productive regions of the Southern Ocean, with maximum NPP estimates  $\sim 1,000 \text{ mg C m}^{-2} \text{ d}^{-1}$  (Figure 4b). The SAZ and PAZ display the largest seasonal variability in NPP rates, with seasonal winter to summer amplitudes of  $\sim 600$  and  $400 \text{ mg C m}^{-2} \text{ d}^{-1}$ , respectively. The SIZ shows a seasonal amplitude similar to the PAZ, and it is the region with the lowest NPP estimates, with summer maxima of  $\sim 400 \text{ mg C m}^{-2} \text{ d}^{-1}$  (Figure 4b), and a net primary productivity  $< 100 \text{ mg C m}^{-2} \text{ d}^{-1}$  during winter months (May–July), with minimum NPP rates of  $\sim 25 \text{ mg C m}^{-2} \text{ d}^{-1}$ .

We quantify the impact of Southern Ocean winter retrievals obtained by the CALIOP sensor on inferred NPP by applying a no-data mask to the merged-based (CALIOP and MODIS) NPP product, analogous to regions of missing oceanic retrievals in  $\text{Chl}_{\text{MODIS}}$  (referred to as MODIS-simulated product). By conducting this simple comparison, we assess differences in NPP estimates induced by the distinct geographical coverage of our merged-based NPP product and a MODIS-only product. Mean monthly NPP retrievals based on merged CALIOP and MODIS information are obtained throughout the full annual cycle in at least 50% of  $1^\circ$  by  $1^\circ$  grid points in the STZ, SAZ, and PAZ (Figure 4b, open symbols). The MODIS-simulated NPP product retrievals (Figure 4b, black-filled circles) fail to cover at least 50% of grid points of the SAZ during June, and 50% of grid points of the PAZ for the period May–July. The STZ is the most equatorward region, and sufficient retrievals from both MODIS-simulated masked NPP and the unmasked merged-based NPP product can be obtained throughout the full annual cycle. The amount of satellite-based NPP estimates inferred from both products is considerably reduced in the SIZ. In this region, we are only able to obtain mean monthly merged-based NPP over the entire annual cycle by lowering the threshold of available grid points with data to 5%. Applying the same criteria to the MODIS-simulated product, monthly NPP estimates are obtained between September and April. Any increase in the threshold fraction of available grid points with data in this region ( $\geq 10\%$ ), results in a considerable reduction in the number of months with mean NPP estimates from both products.

The fraction of regionally integrated NPP that is unaccounted for by the MODIS-simulated product relative to the unmasked merged-based NPP reaches a maximum of 61% during June in the PAZ (Figure 5a). In June, solar angles are lowest in the southern hemisphere, and unaccounted NPP by the MODIS-simulated product is highest in all regions of the Southern Ocean. The PAZ, followed by the SAZ, are the regions with the greatest difference in regionally integrated NPP between the MODIS-simulated product and the merged-based NPP estimate. These differences are mainly restricted to winter (low solar angle) months (May–July). As mentioned above, the STZ has MODIS coverage over the entire annual cycle, and thus, no difference between products is found for this region. We do not quantify the amount of unaccounted NPP in the SIZ due to the consistent low amount of retrievals from both products throughout the full annual cycle in this region.

Overall, the amount of unaccounted regionally integrated NPP over the full annual cycle is less than 12% for the whole Southern Ocean and any of its environmental regions (Figure 5a, annual). This represents  $0.24 \text{ Pg C yr}^{-1}$  of unaccounted NPP over the entire Southern Ocean. The PAZ and SAZ are the major contributors

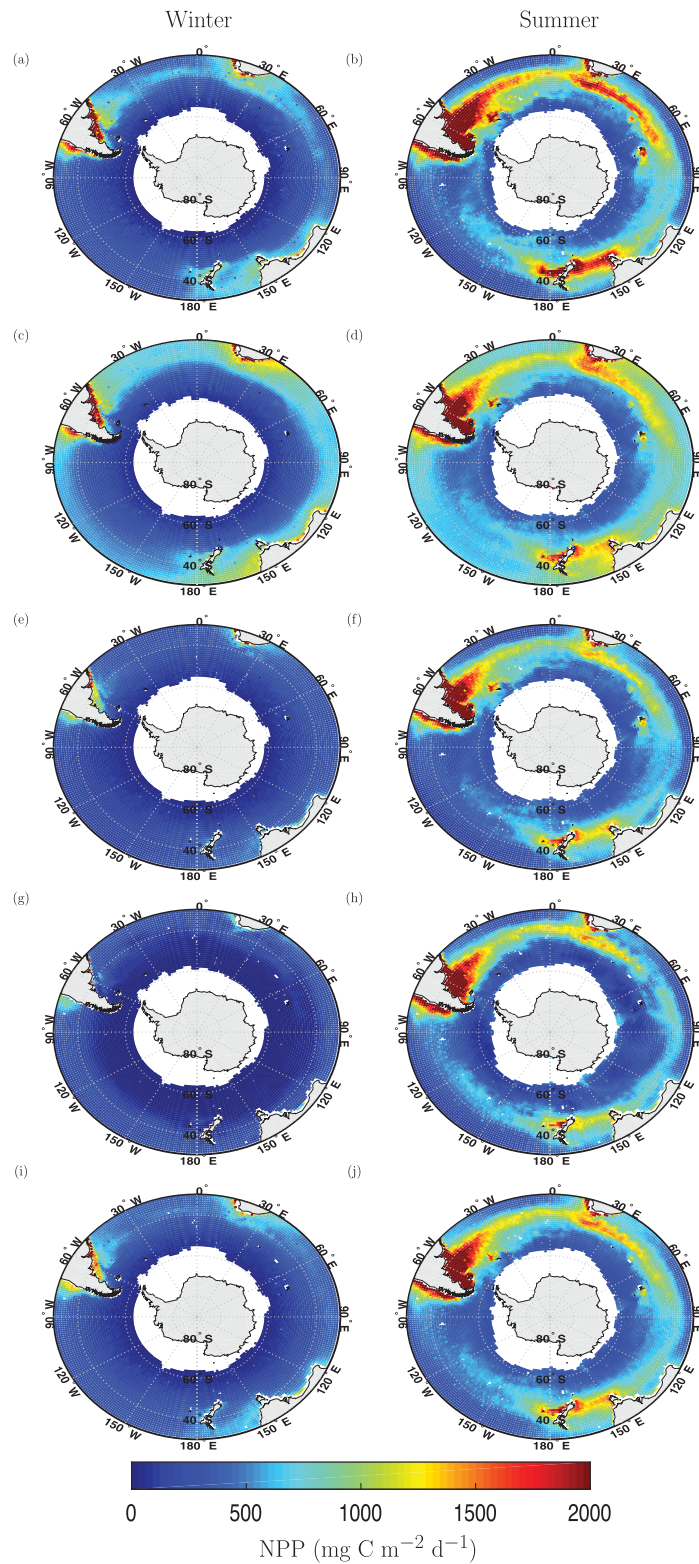


**Figure 3.** Mean Southern Ocean net primary production from satellite-based Chl, phytoplankton carbon, and Chl:C estimates for austral winter (May–July) and summer (November–January) inferred by the (a, b) VGPM, (c, d) Marra03, (e, f) Carr02, (g, h) CbPM05, and (i, j) the mean of the four productivity models. NPP estimates represent mean conditions of the period 2006–2015.



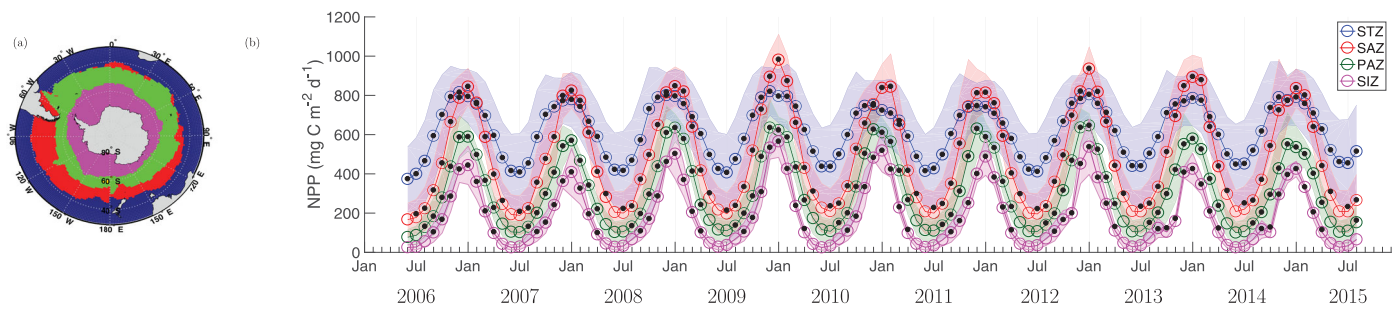


**Figure 4.** (a) Environmental regions of the Southern Ocean based on 2004–2014 Argo climatology of temperature and salinity (Roemmich & Gilson, 2009), following the criteria of Orsi et al. (1995): STZ (blue), SAZ (red), PAZ (green), and SIZ (magenta). (b) Satellite-based monthly NPP obtained from the average of the four productivity models ( $\pm$  standard deviation) for the areal mean of the four environmental regions defined for the Southern Ocean in (a). Open circles connected by color lines represent estimates obtained by the unmasked merged (CALIOP and MODIS) NPP product. Black-filled circles shows monthly estimates from the MODIS-simulated no data masked product. Estimates for the STZ (blue), SAZ (red), and PAZ (green), are shown when  $\geq 50\%$  of  $1^\circ$  by  $1^\circ$  grid boxes within each environmental region have NPP data. For the SIZ (magenta), symbols are present when  $\geq 5\%$  of grid boxes have NPP data.

to this difference, with  $0.17$  and  $0.07 \text{ Pg C yr}^{-1}$ , respectively, while no appreciable difference is found for the STZ (Figure 5b). Our regional satellite-based NPP estimates are difficult to compare against previous studies due to different criteria employed to define environmental regions in the Southern Ocean (Arrigo et al., 1998, 2008). Our mean annual NPP integrated for the oceanic area south of  $30^\circ\text{S}$  is  $15.8 (\pm 3.9, \text{ standard deviation of NPP models}) \text{ Pg C yr}^{-1}$ . Mean annual NPP integrated for the region south of  $50^\circ\text{S}$  is  $2.7 (\pm 0.6) \text{ Pg C yr}^{-1}$ . Inferred NPP for the region south of  $50^\circ\text{S}$  is in the same range of previous estimates of  $1.9$  (period 1997–2006; Arrigo et al., 2008),  $2.9$  (period 1997–1998; Moore & Abbott, 2000), and  $1.5 \text{ Pg C yr}^{-1}$  (period 2003–2007; Shang et al., 2010) for the same area (Table 1).

### 3.3. Export Efficiency in the Southern Ocean

We obtain estimates of carbon export efficiency for the Southern Ocean from the five empirical models described in section 2.4, forced with satellite net primary production estimates (mean of NPP models), Chl, SST, and a climatology of surface  $[\text{Si}]$  (according to the variables required by each e-ratio model) (Figure 6). These models show important differences in the mean climatological patterns of inferred e-ratio for the Southern Ocean. Over the entire Southern Ocean, equation Britten17 and equation SO predict the highest e-ratios ( $>0.4$ ). Nevertheless, there are important sub-regional differences in the estimation of the e-ratio by the different empirical models. Equation Dunne05 and Laws11 predict the highest e-ratios in low Southern Ocean latitudes,  $\sim$  north of  $50^\circ\text{S}$ . Estimates of e-ratio from equation Dunne05 begin to increase southward of  $40^\circ\text{S}$ , where NPP and Chl are highest. A similar but less pronounced pattern is observed in estimates from equation Laws11, particularly in the highly productive region east of South America, in the Atlantic ocean. Equation Britten17 predicts the highest e-ratios, where export efficiency increases with latitude. Highest e-ratios from this equation are found southward of  $50^\circ\text{S}$  due to a combination of low NPP, low SST, and high  $[\text{Si}]$ . Equation SO also shows a clear latitudinal increase from predicted low e-ratios in lower latitudes (north of  $50^\circ\text{S}$ , e-ratio  $< 0.2$ ), to high e-ratios toward higher latitudes (south of  $50^\circ\text{S}$ , e-ratio  $> 0.4$ ). Inferred patterns of export efficiency are associated with the distinct relationships between e-ratio, NPP, and biomass (Chl) in each of these models. Equation Dunne05 suggests a positive relationship between e-ratio and Chl, and equation Laws11 suggest a positive relationship between e-ratio and NPP. Hence, these equations predict a distribution of e-ratios that is positively associated with patterns of net primary production. Conversely, equation Britten17 and equation SO suggest an inverse relationship between export efficiency and primary productivity, resulting in low inferred e-ratios between  $40^\circ$ – $60^\circ\text{S}$ . Equation Henson11 predicts overall the lowest e-ratios in the Southern Ocean. This formulation is likely over-simplistic for the estimation of the e-ratio (Henson et al., 2015). All of these models account to some degree for a negative relationship between export efficiency and temperature (equation Henson11 depends on this empirical relationship alone). The inverse relationship between e-ratio and temperature is the driving mechanism of increasing e-ratios with increasing latitude, observed in the output from all five models (to a lesser extent in equation Laws11). Equation Britten17 shows the highest e-ratios because it also accounts for the ballasting effect of Si.

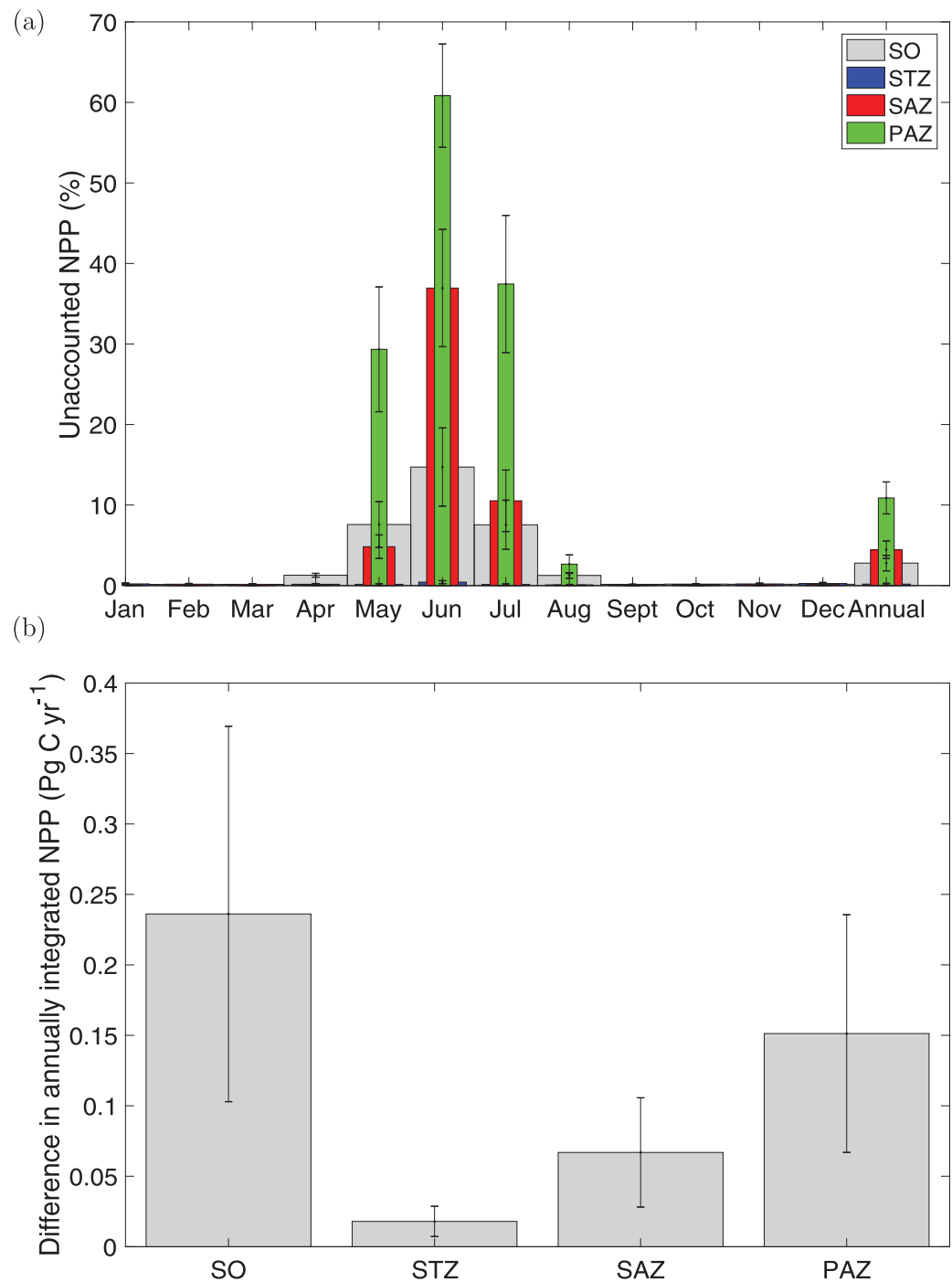


**Figure 5.** (a) Proportion of unaccounted NPP (%) by MODIS-simulated no data masked with respect to the unmasked merged (CALIOP and MODIS) NPP product  $\left(\frac{\text{MODIS-simulated} \times 100}{\text{unmasked CALIOP NPP}}\right)$  in monthly and annually, regionally integrated NPP rates for the STZ, SAZ, PAZ, and over the entire Southern Ocean (south of 30°S) (SO) (2006–2015 annual climatology) (unaccounted NPP in the SIZ is not quantified due to the consistent low amount of retrievals from both products throughout the full annual cycle in this region). (b) Difference in annually integrated NPP for the whole Southern Ocean and each environmental region between unmasked and masked NPP products (unmasked merged NPP - MODIS-simulated no data masked) for the 2006–2015 climatology. The 2006–2015 climatology is derived from monthly mean NPP maps, from June 2006 to August 2015. In both plots, estimates represent the average ( $\pm$  standard deviation) of the four productivity models used in this study (VGPM, Marra03, Carr02, and CbPM05).

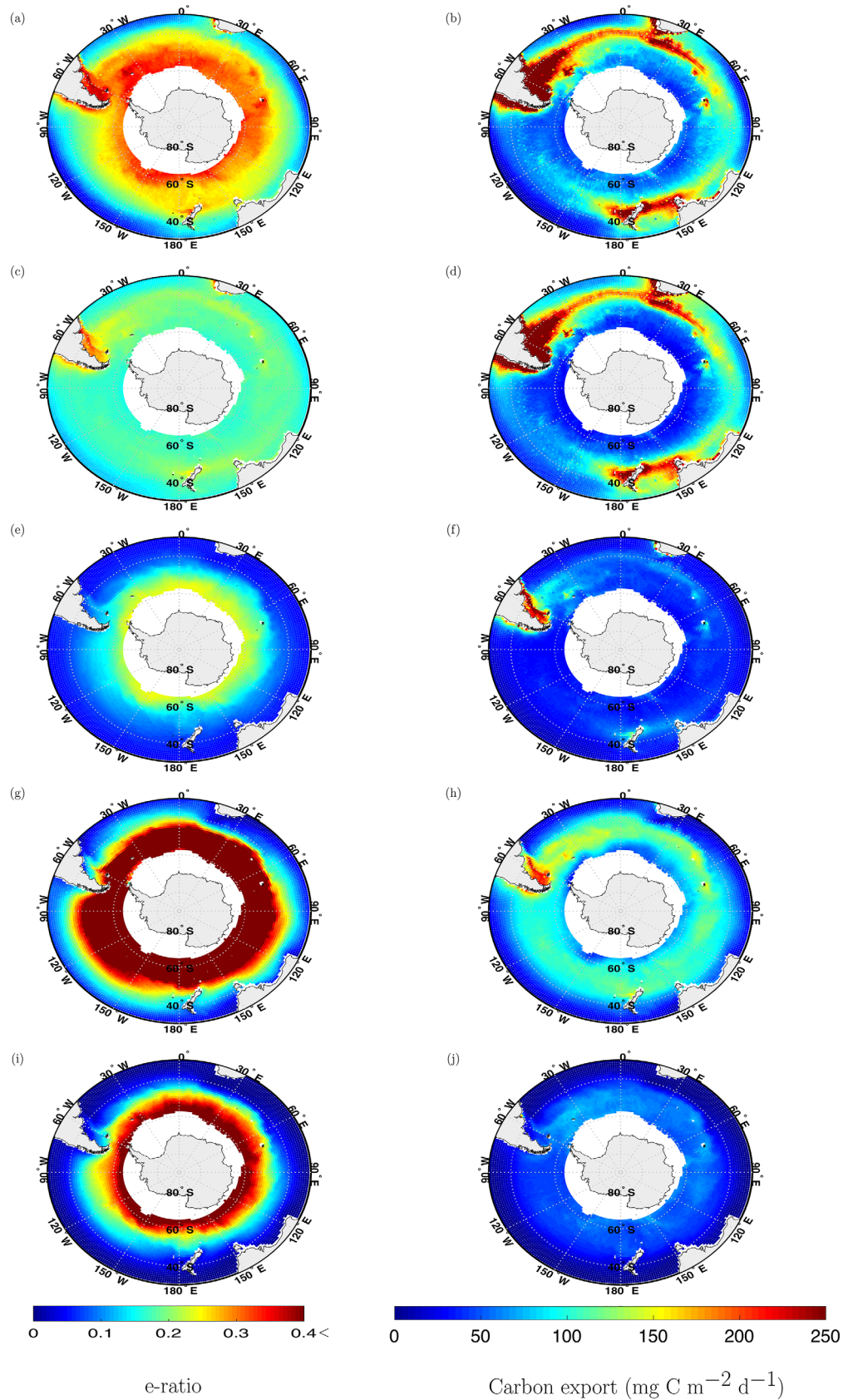


Figure 6. (continued)

Seasonal estimates of e-ratios from each of these models also show contrasting behaviors (Figure 7). In the STZ, e-ratio estimates from all models are relatively low ( $< 0.3$ ), and highest e-ratios are predicted during austral winter. This seasonal trend is mainly driven by the negative relationship between export efficiency and temperature, which is present in all models. In the other three regions (SAZ, PAZ, and SIZ), the seasonal amplitude of NPP is larger, resulting in an opposite seasonality of predicted maximum and minimum e-ratios from the different models. Equation Dunne05 and Laws11 show highest estimates during austral summer months, when primary productivity and biomass are highest. By contrast, equation Britten17 and equation SO predict the highest e-ratios during winter, when NPP is lowest. Equation Henson11 shows little seasonal variability, driven only by seasonal changes in temperature. Overall, the highest e-ratios are predicted by equation Britten17, particularly in the PAZ and SIZ, where export efficiency during austral winter can be as high as 0.8. This is due to a combination of low temperature and low NPP. Equation SO shows a similar increase from the STZ to the SIZ, but the overall magnitude of predicted e-ratios is lower than equation Britten17. This is because equation SO accounts for the negative relationship between e-ratio and NPP, but not for the ballasting effect induced by Si utilization (Britten et al., 2017). The divergent patterns in export efficiency obtained from each of these models have significant impacts on predicted carbon export rates in the Southern Ocean.

### 3.4. Implications for Organic Carbon Export

Organic carbon export is computed as the product of satellite-based NPP (mean of NPP models) and the e-ratio obtained from each of the five models described in section 2.4. Differences in the climatological mean estimates of organic carbon export resulting from each of the five models are large (Figure 6). Equation Dunne05 and equation Laws11 show the highest estimates of carbon export, with rates  $> 250 \text{ mg C m}^{-2} \text{ d}^{-1}$  in the productive band between  $40^{\circ}$ – $50^{\circ}$ S, which covers most basins of the Southern Ocean, except for the eastern Pacific. The spatial pattern of inferred carbon export from these two models is very similar to that of NPP (Figure 3). By contrast, models that have an inverse relationship between e-ratio and NPP (equation Britten17 and SO) show reduced spatial variability and lower export rates. Equation Britten17 shows a flat spatial distribution of export rates, varying from 100 to  $200 \text{ mg C m}^{-2} \text{ d}^{-1}$  between  $40^{\circ}$ – $60^{\circ}$ S. North of  $40^{\circ}$  and close to the ice margin, predicted carbon export from this model is  $< 100 \text{ mg C m}^{-2} \text{ d}^{-1}$ . Equation SO predicts export rates  $< 80 \text{ mg C m}^{-2} \text{ d}^{-1}$  throughout the entire Southern Ocean. Equation Henson11 (which only depends on temperature) also shows reduced spatial variability in carbon export, with rates of  $\sim 50 \text{ mg C m}^{-2} \text{ d}^{-1}$  in most of the Southern Ocean, with the exception of regions of high primary productivity and high inferred phytoplankton biomass (Figures 2 and 3), where estimates of carbon export can be up to  $200 \text{ mg C m}^{-2} \text{ d}^{-1}$ .

Differences between models are also evident in predicted monthly estimates of carbon export for the different environmental regions defined for the Southern Ocean (Figure 8). Equation Dunne05 and Laws11 show high seasonality and the highest summer export rates, particularly in the SAZ, where inferred carbon export varies between 50 and  $350 \text{ mg C m}^{-2} \text{ d}^{-1}$ . Equation Britten17 and equation SO show reduced seasonal variability and higher winter export rates than the other models in the PAZ and SIZ. Equation Henson11 also shows low seasonality and low export rates, with maximum estimates  $\sim 100 \text{ mg C m}^{-2} \text{ d}^{-1}$  in the SIZ.

A clear pattern emerges from the comparison of carbon export rates in the Southern Ocean derived from the five empirical models of export efficiency used in this study: Models that account for a positive relationship between e-ratio and Chl, or e-ratio and NPP, show the highest rates and the largest seasonal and spatial variability in inferred export rates (Dunne05, Laws11). In contrast, models that account for an inverse relationship between e-ratio and NPP (equation Britten17 and equation SO) or ignore any relationship between these variables (equation Henson11), predict in general lower export rates and a more homogeneous spatial pattern of carbon export in the Southern Ocean.

**Figure 6.** Mean annual export efficiency (e-ratio) and derived carbon export rates in the Southern Ocean (computed as the product of e-ratio and satellite-based NPP) predicted by the five empirical models of export efficiency evaluated in this study: (a and b) Dunne05, (c and d) Laws11, (e and f) Henson11, (g and h) Britten17, and (i and j) SO. Estimates are obtained for the 2006–2015 annual climatology of satellite-based Chl and NPP, MODIS SST, and WOA13 Si climatology. Outputs are obtained for the mean of the four productivity models used in this study (VGPM VGPM, Marra03, Carr02, and CbPM05).

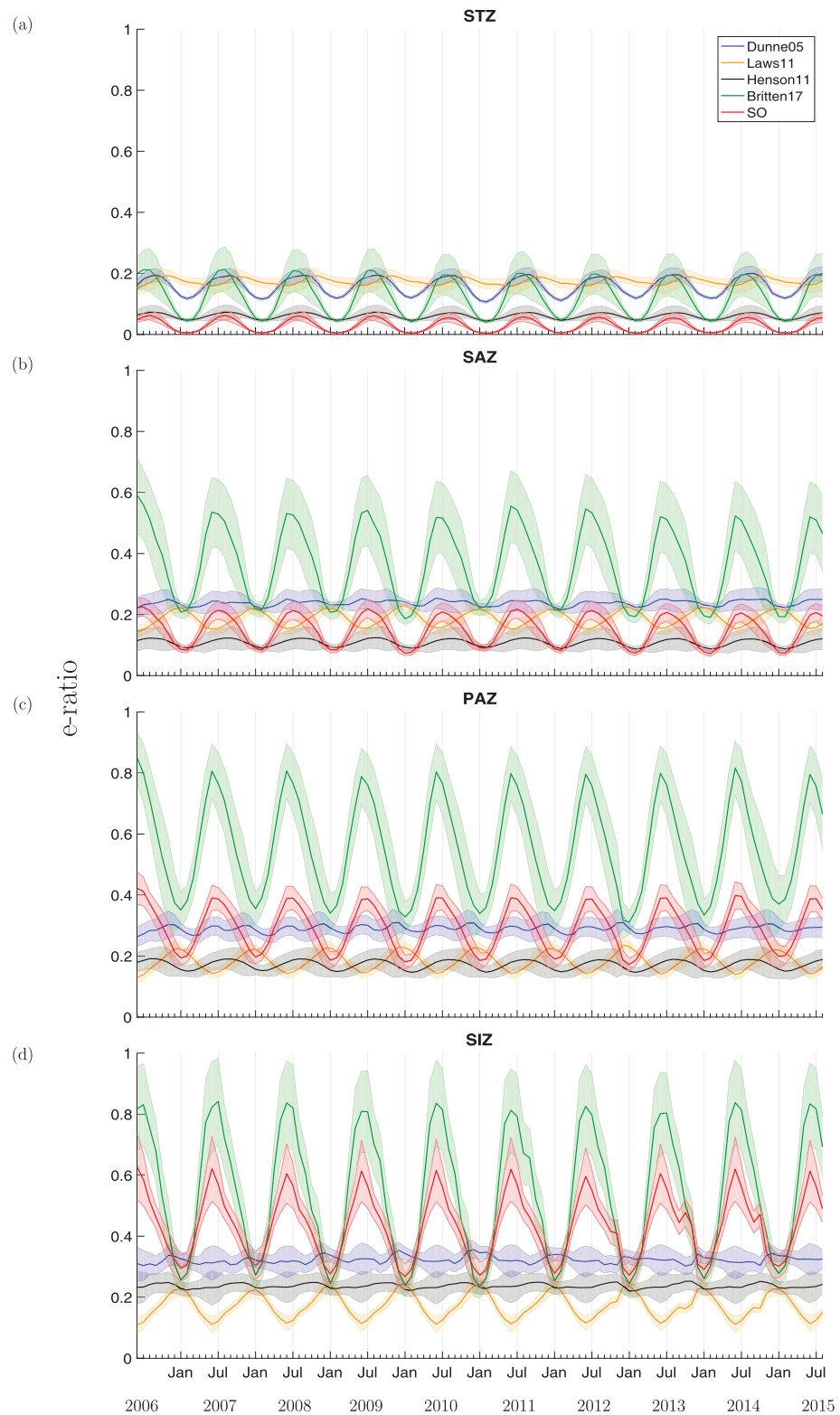


**Figure 7.** Mean monthly e-ratio estimates obtained from the five empirical models of export efficiency evaluated in this study for each of the environmental regions defined in the Southern Ocean: (a) STZ, (b) SAZ, (c) PAZ, and (d) (SIZ). Estimates represent the average ( $\pm$  standard deviation, shaded area) output of the four productivity models used in this study.

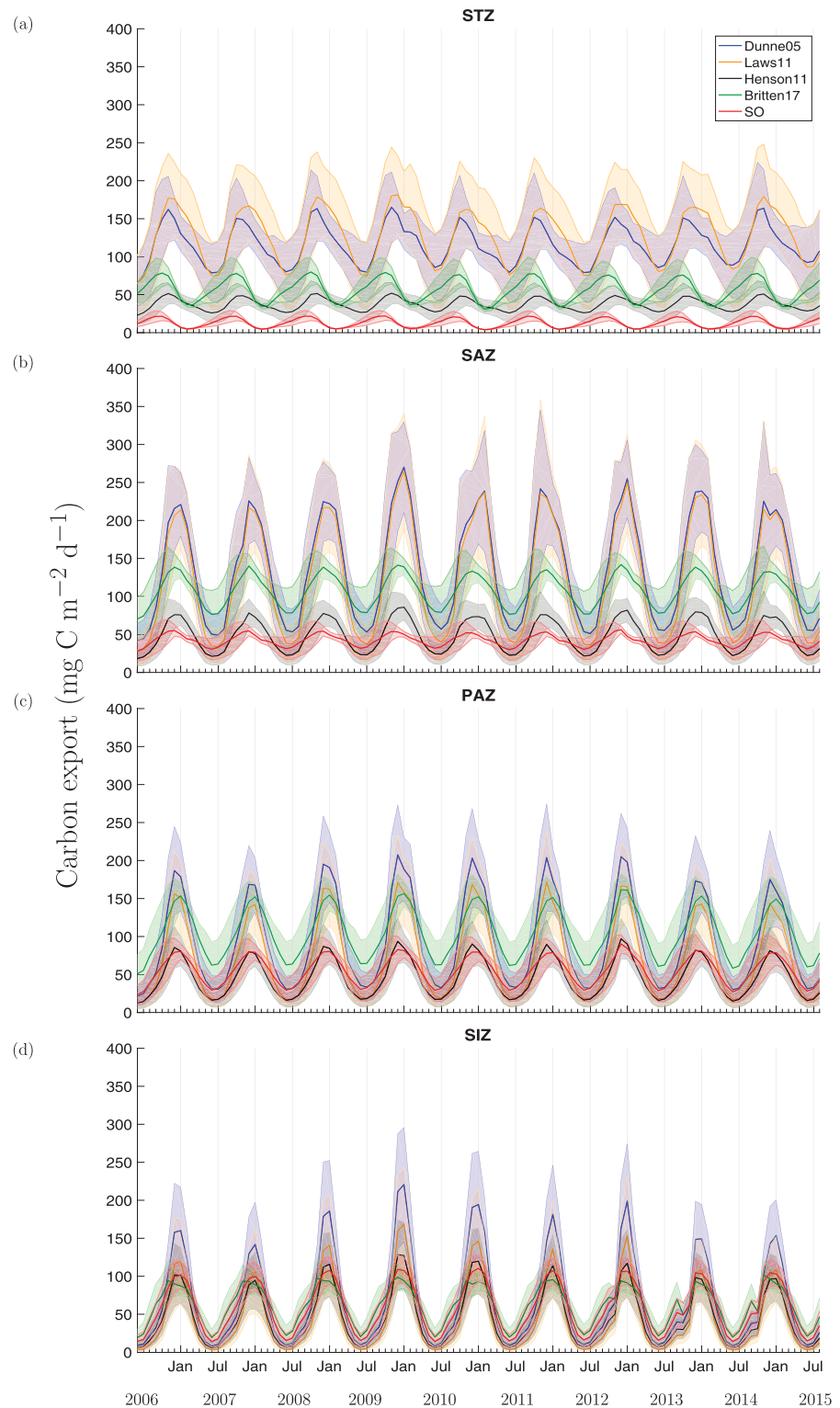


**Figure 8.** Mean monthly estimates of carbon export ( $\text{mg C m}^{-2} \text{d}^{-1}$ ) predicted as the product of satellite-based NPP and e-ratio obtained from the five empirical models of export efficiency evaluated in this study for each of the environmental regions defined in the Southern Ocean: (a) STZ, (b) SAZ, (c) PAZ, and (d) (SIZ). Estimates represent the average ( $\pm$  standard deviation, shaded area) output of the four productivity models used in this study.

### 3.5. Differences in Annual Carbon Export

We compare the climatological zonal mean annual carbon export ( $\text{mol C m}^{-2} \text{yr}^{-1}$ ) inferred from the five export efficiency models, and a compilation of in situ-based estimates of annual net community production (ANCP) largely composed by profiling floats observations as part of the SOCCOM program (Johnson et al., 2017) (Figure 9). Under steady-state conditions (i.e., no net accumulation/loss of organic carbon), carbon export should equal net community production (NCP) in the upper productive oceanic layer, where NCP represents the net production of organic carbon after accounting for the respiration needs of the autotrophic and heterotrophic components of the ecosystem (Ducklow & Doney, 2013). Thus, assuming that most of the organic carbon exported out of the surface ocean over the annual cycle is in the form of particles, estimates of ANCP and carbon export should converge. The ANCP estimates include observations of nitrate drawdown/consumption in the productive layer (Johnson et al., 2017; Lourey & Trull, 2001; MacCready & Quay, 2001), time series analysis of dissolved nutrients, dissolved inorganic carbon (DIC), and surface ocean  $\text{pCO}_2$  (Bender & Jönsson, 2016; McNeil & Tilbrook, 2009; Munro et al., 2015; Shadwick et al., 2015), and changes in mesopelagic oxygen inventory (Hennon et al., 2016; Martz et al., 2008; Riser & Johnson, 2008). ANCP estimates are binned and averaged by  $5^\circ$  latitudinal bands. These observations indicate ANCP (carbon export)  $< 1 \text{ mol C m}^{-2} \text{yr}^{-1}$  ( $12 \text{ gr C m}^{-2} \text{yr}^{-1}$ ), between  $20^\circ\text{S}$  and  $35^\circ\text{S}$ , an increase in export to  $\sim 3 \text{ mol C m}^{-2} \text{yr}^{-1}$  ( $36 \text{ gr C m}^{-2} \text{yr}^{-1}$ ) between  $40^\circ\text{S}$  and  $50^\circ\text{S}$ , and a subsequent decline in export to  $\sim 1.5 \text{ mol C m}^{-2} \text{yr}^{-1}$  ( $18 \text{ gr C m}^{-2} \text{yr}^{-1}$ ), south of  $60^\circ\text{S}$ . Our empirical model-based estimates predict certain features of this latitudinal pattern, with clear differences in the magnitude of exported carbon between models. Models

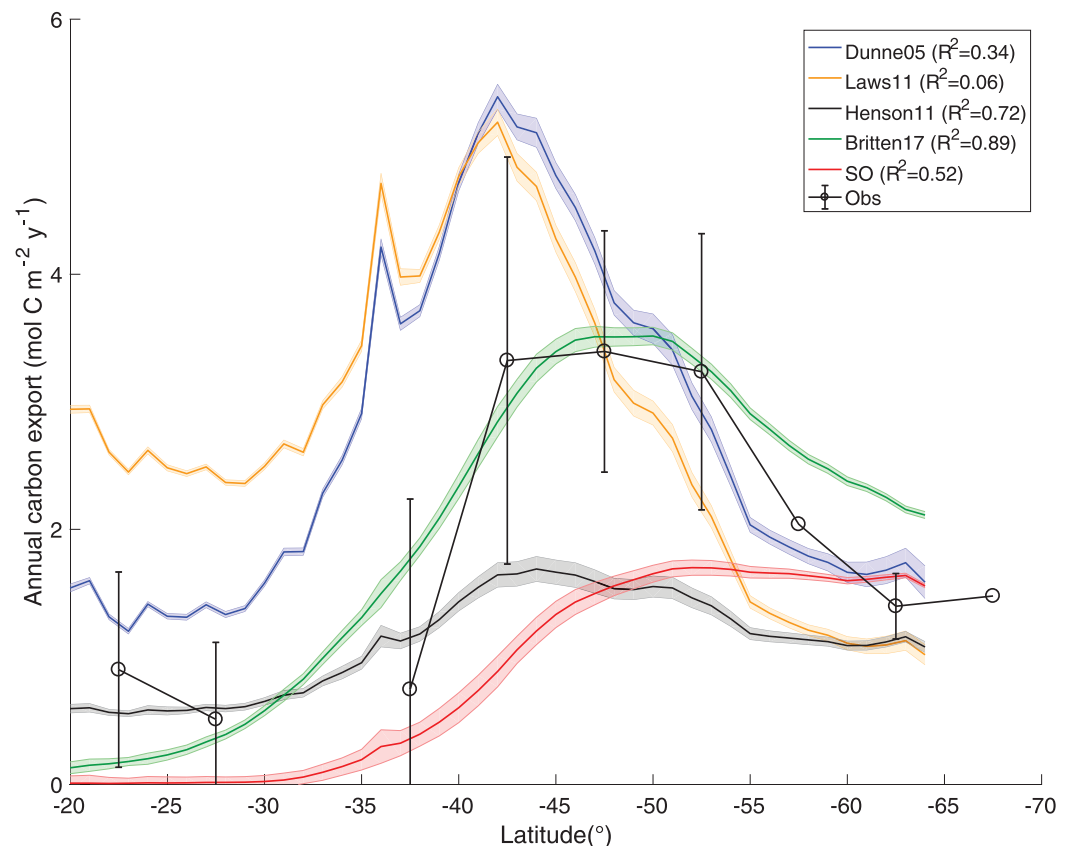


**Figure 9.** Zonal mean annual carbon export ( $\text{mol C m}^{-2} \text{yr}^{-1}$ ) computed as the product of satellite-based NPP and e-ratio obtained from the five empirical models of export efficiency evaluated in this study. Model estimates (continuous solid line) represent the average ( $\pm$  standard deviation, shaded area) output of the four productivity models used in this study. Also shown are in situ estimates (Obs) of ANCP from multiple methods compiled by Johnson et al. (2017) and binned (averaged) by  $5^\circ\text{S}$  latitudinal bands ( $\pm$  Error bars at 90% confidence intervals based on the standard deviation of all data in each band). There are no in situ-based ANCP observations between  $30^\circ\text{S}$  and  $35^\circ\text{S}$  in the data set of Johnson et al. (2017).  $R^2$  between models and observations is computed over the entire latitudinal range, applying a linear interpolation between the in situ-based ANCP estimates.

that account for a positive relationship between e-ratio and Chl (equation Dunne05), and e-ratio and NPP (equation Laws11), predict the highest estimates of carbon export north of 50°S. Models that have an inverse relationship between e-ratio and NPP (equation Britten17 and equation SO) yield lower annual export rates north of 50°S. Equation Britten17 agrees well within the range of uncertainty of situ-based estimates of ANCP over most of the latitudinal range between 20°S and 70°S. We calculate the coefficient of determination ( $R^2$ ) between models and observations over the entire latitudinal range, applying a linear interpolation between the in situ-based ANCP estimates (Figure 9). Equation Britten17 presents the largest agreement with observations,  $R^2 = 0.89$ , followed by equation Henson11, with an  $R^2 = 0.72$ , and equation SO with  $R^2 = 0.52$ . Equation Britten17 and equation SO are similar in the sense that both have an inverse relationship between e-ratio and NPP, and both are constrained by data on export, temperature, and NPP exclusively for the Southern Ocean (Maiti et al., 2013).

The larger agreement between equation Britten17 and in situ-based ANCP estimates (compared to equation SO) is likely due the inclusion of [Si] in this empirical model, which accounts for the enhancement of vertical particle flux caused by the ballasting effect associated with inorganic minerals (Armstrong et al., 2001; Sanders et al., 2010). The compilation of export efficiency estimates for the Southern Ocean from Maiti et al. (2013) suggests a reduced dependency of the e-ratio on temperature with respect to global observations (Dunne et al., 2005; Laws et al., 2000). Britten et al. (2017) re-analyze the data compilation of Maiti et al. (2013) and showed that the effect of temperature on the regulation of the e-ratio is obscured by the offsetting interaction of temperature-driven respiration and silica ballast. Silica-rich waters upwell in the Southern Ocean and travel northward (Sarmiento et al., 2004a). During this trajectory, high [Si] promotes particle export, while increase surface warming during the northward trajectory enhances respiration of organic matter. This leads to a counteracting effect between [Si] and temperature on export efficiency. Equation Britten17 reveals the inverse effect of temperature on the e-ratio once silica ballast is accounted for. This mechanism is particular for the Southern Ocean, and thus, does not imply that equation Britten17 would yield accurate e-ratio estimates in other regions.

Differences between estimates of integrated annual carbon export for the Southern Ocean (south of 30°S) vary by a factor of  $\sim 3$  (Figure 10). Our best estimate of carbon export for the Southern Ocean (based on the comparison with observations of ANCP) is that of equation Britten17 =  $2.7 (\pm 0.6)$  Pg C yr<sup>-1</sup>. Global estimates of carbon export cluster around 10 Pg C yr<sup>-1</sup> (DeVries & Weber, 2017; Dunne et al., 2005; Laws et al.,

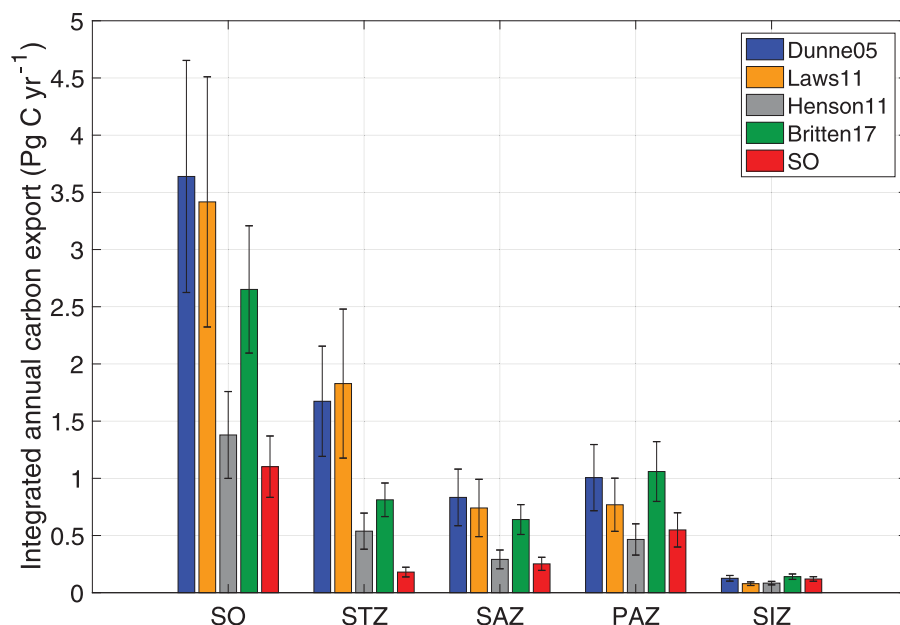


**Figure 10.** Regionally integrated annual carbon export (Pg C yr<sup>-1</sup>) for the Southern Ocean (south of 30°S) (SO) and each of the environmental regions, inferred from each of the five empirical models of export efficiency evaluated in this study. Estimates represent the average ( $\pm$  standard deviation) output of the four productivity models used in this study.



2000; Schlitzer, 2002), and  $5 \text{ Pg C yr}^{-1}$  (Henson et al., 2011; Siegel et al., 2014). In this context, our best estimate for the Southern Ocean represents  $\sim 25\%$ , and  $50\%$  of the global organic carbon exported from the surface ocean, respectively. Equation Dunne05 and Laws11 predict the highest estimates of carbon export in the Southern Ocean ( $> 3 \text{ Pg C yr}^{-1}$ ), while equation Henson11 and equation SO predict the lowest rates ( $> 1.5 \text{ Pg C yr}^{-1}$ ). The difference between model estimates is highest in the STZ and SAZ, where NPP is highest. Regionally integrated estimates of carbon export from the different models converge toward SIZ, where differences in empirical e-ratio models used to estimate carbon export are negligible due to overall low net primary productivity rates in this region.

### 3.6. How to Interpret the Inverse Relationship Between Export Efficiency and Primary Productivity in the Southern Ocean?

A problematic feature in the Southern Ocean observations compiled by Maiti et al. (2013), is that there is no obvious relationship between carbon export and NPP (the relationship is highly scattered, Supporting information Figure S2). Given that the e-ratio is defined as the ratio of export production:NPP, and there is no clear relationship between these variables (i.e., export production and NPP), a possible interpretation of the inverse e-ratio versus NPP relationship, is that it is spurious (Atchley et al., 1976; Pearson, 1896). Ratios are problematic for statistical analysis (Packard & Boardman, 1988). Given that NPP is involved in both the independent variable "X" ( $X = \text{NPP}$ ), and the dependent variable "Y" ( $Y = \text{e-ratio} = \frac{\text{export production}}{\text{NPP}}$ ), as NPP becomes larger, there would be a tendency for  $\frac{\text{export production}}{\text{NPP}}$  to become smaller (Berges, 1997). This statistical difficulty does not necessarily invalidate the observation of an inverse e-ratio versus NPP relationship (Prairie & Bird, 1989). There could be real biogeochemical mechanisms preventing the emergence of a positive relationship between export production and NPP in the Southern Ocean, which could be interpreted as a decrease in export efficiency with increased primary productivity (Cavan et al., 2017). Given the good agreement of equation Britten17 with the in situ-based ANCP observations, we believe that there is descriptive value in the data of Maiti et al. (2013), particularly when combined with information from surface Si concentration.

To our knowledge, this problematic feature has not been considered in previous studies of export efficiency in the Southern Ocean. Perhaps the most unambiguous way forward is to analyze directly the relationship (or lack thereof) between carbon export and primary productivity, and/or by aiming to explain observed patterns in export efficiency from environmental variables different from export and NPP.

## 4. Conclusions

By combining novel lidar (CALIOP) data of ocean particulate backscattering with information from a passive satellite sensor (MODIS), we infer mean monthly phytoplankton biomass (Chl and C<sub>phyto</sub>) and NPP estimates for the Southern Ocean over the entire annual cycle for the period June 2006 to August 2015. Mean monthly NPP estimates in the Southern Ocean are highest in the STZ ( $400\text{--}800 \text{ mg C m}^{-2} \text{ d}^{-1}$ ) and SAZ ( $200\text{--}1,000 \text{ mg C m}^{-2} \text{ d}^{-1}$ ), and lowest in the PAZ ( $100\text{--}600 \text{ mg C m}^{-2} \text{ d}^{-1}$ ) and SIZ ( $25\text{--}400 \text{ mg C m}^{-2} \text{ d}^{-1}$ ). Our mean annual NPP integrated for the oceanic area south of  $30^\circ\text{S}$  is  $15.8 (\pm 3.9, \text{ standard deviation of NPP models}) \text{ Pg C yr}^{-1}$ . Mean annual NPP integrated for the oceanic region south of  $50^\circ\text{S}$  is  $2.7 \text{ Pg C yr}^{-1} (\pm 0.6)$ , which agrees within the uncertainty of previous estimates. Using our satellite-based NPP rates, we assess carbon export estimates from five different empirical models of export efficiency constrained by different relationships between Chl, NPP, temperature, surface Si concentration, and e-ratio. A key distinction between these formulations is their empirical relationship between export efficiency and primary productivity. Models with a negative e-ratio versus NPP relationship predict a latitudinal increase in export efficiency in the Southern Ocean. Equation Britten17, which accounts for the silica-induced ballasting effect, estimates considerably high e-ratios ( $> 0.4$ ) south of  $50^\circ\text{S}$ . Models that have an inverse e-ratio versus NPP relationship, or that depend only on temperature as a predictor of e-ratio, estimate a reduced spatial variation in carbon export, in line with recent observationally constrained estimates (Emerson, 2014). Equation Britten17 agrees well within the uncertainty of mean annual carbon export inferred from in situ-based ANCP estimates in the Southern Ocean. Our results suggest that empirical models based on global observations (equation Dunne05 and equation Laws11) can be biased in the Southern Ocean, predicting annually integrated rates  $\sim 33\%$  higher than our best estimate (equation Britten17 =  $2.7 \text{ Pg C yr}^{-1}$ ).

Our results agree with recent analysis which indicate that silica-induced ballasting is a key process to take into account for the estimation of carbon export in the Southern Ocean (Britten et al., 2017). It is still not clear, however, what drives an inverse relationship between export efficiency and primary productivity in this region (assuming that this relationship is not entirely driven by a statistical artifact). Recent evidence points to the role of zooplankton in particle grazing and fragmentation as an important mechanism in the regulation of particle export (Cavan et al., 2017). Future efforts should aim to revise mechanistic parameterizations of marine carbon fluxes in ecological models in order to improve our understanding of the processes driving regional differences in carbon export efficiency (e.g., Henson et al., 2015). This will lead to improved reliability in estimates and projections of the efficiency of the biological carbon pump.

#### Acknowledgments

We wish to thank M. Behrenfeld and R. O'Malley for making available the CALIOP  $b_{bp}$  data set. We thank Erik Buitenhuis for sharing the compiled in situ NPP estimates. We would also like to thank Edward Laws for insightful comments during the elaboration of the manuscript. The research leading to these results was partially sponsored by NSF's Southern Ocean Carbon and Climate Observations and Modeling (SOCCOM) Project under the NSF Award PLR-1425989 with additional support from NOAA and NASA Ocean Biology and Biogeochemistry (OBB) program. L. Arteaga was mainly supported by NASA under Award NNX17AI73G. All details and web addresses needed to access the data used to produce our results are described in section 2 of this paper.

#### References

- Armstrong, R. A., Lee, C., Hedges, J. I., Honjo, S., & Wakeham, S. G. (2001). A new, mechanistic model for organic carbon fluxes in the ocean based on the quantitative association of POC with ballast minerals. *Deep Sea Research Part II: Topical Studies in Oceanography*, 49(1), 219–236. [https://doi.org/10.1016/S0967-0645\(01\)00101-1](https://doi.org/10.1016/S0967-0645(01)00101-1)
- Arrigo, K. R., van Dijken, G. L., & Bushinsky, S. (2008). Primary production in the southern ocean, 1997–2006. *Journal of Geophysical Research*, 113, C08004. <https://doi.org/10.1029/2007JC004551>
- Arrigo, K. R., Worthen, D., Schnell, A., & Lizotte, M. P. (1998). Primary production in southern ocean waters. *Journal of Geophysical Research: Oceans*, 103(C8), 15587–15600. <https://doi.org/10.1029/98JC00930>
- Arteaga, L., Pahlow, M., & Oschlies, A. (2016). Modeled chl: ratio and derived estimates of phytoplankton carbon biomass and its contribution to total particulate organic carbon in the global surface ocean. *Global Biogeochemical Cycles*, 30, 1791–1810. <https://doi.org/10.1002/2016GB005458>
- Atchley, W. R., Gaskins, C. T., & Anderson, D. (1976). Statistical properties of ratios. i. empirical results. *Systematic Biology*, 25(2), 137–148. <https://doi.org/10.2307/2412740>
- Behrenfeld, M. J., Boss, E., Siegel, D. A., & Shea, D. M. (2005). Carbon-based ocean productivity and phytoplankton physiology from space. *Global Biogeochemical Cycles*, 19, GB1006. <https://doi.org/10.1029/2004GB002299>
- Behrenfeld, M. J., & Falkowski, P. G. (1997). Photosynthetic rates derived from satellite-based chlorophyll concentration. *Limnology and Oceanography*, 42(1), 1–20. <https://doi.org/10.4319/lo.1997.42.1.0001>
- Behrenfeld, M. J., Hu, Y., Hostetler, C. A., Dall'olmo, G., Rodier, S. D., Hair, J. W., & Trepte, C. R. (2013). Space-based lidar measurements of global ocean carbon stocks. *Geophysical Research Letters*, 40, 4355–4360. <https://doi.org/10.1002/grl.50816>
- Behrenfeld, M. J., Hu, Y., O'Malley, R. T., Boss, E. S., Hostetler, C. A., Siegel, D. A., et al. (2017). Annual boom-bust cycles of polar phytoplankton biomass revealed by space-based lidar. *Nature Geoscience*, 10, 118–122. <https://doi.org/10.1038/ngeo2861>
- Behrenfeld, M. J., Marañón, E., Siegel, D. A., & Hooker, S. B. (2002). Photoacclimation and nutrient-based model of light-saturated photosynthesis for quantifying oceanic primary production. *Marine Ecology Progress Series*, 228, 103–117.
- Behrenfeld, M. J., O'Malley, R. T., Boss, E. S., Westberry, T. K., Graff, J. R., Halsey, K. H., et al. (2016). Reevaluating ocean warming impacts on global phytoplankton. *Nature Climate Change*, 6(3), 323–330. <https://doi.org/10.1038/nclimate2838>
- Bender, M. L., & Jönsson, B. (2016). Is seasonal net community production in the south pacific subtropical gyre anomalously low? *Geophysical Research Letters*, 43, 9757–9763. <https://doi.org/10.1002/2016GL070220>
- Berges, J. A. (1997). Ratios, regression statistics, and spurious correlations. *Limnology and Oceanography*, 42(5), 1006–1007. <https://doi.org/10.4319/lo.1997.42.5.1006>
- Boyd, P. W., Jickells, T., Law, C. S., Blain, S., Boyle, E. A., Buesseler, K. O., et al. (2007). Mesoscale iron enrichment experiments 1993–2005: Synthesis and future directions. *Science*, 315, 612–617. <https://doi.org/10.1126/science.1131669>
- Britten, G. L., Wakamatsu, L., & Primeau, F. W. (2017). The temperature-ballast hypothesis explains carbon export efficiency observations in the southern ocean. *Geophysical Research Letters*, 44, 1831–1838. <https://doi.org/10.1002/2016GL072378>
- Buitenhuis, E. T., Hashioka, T., & Quéré, C. L. (2013). Combined constraints on global ocean primary production using observations and models. *Global Biogeochemical Cycles*, 27, 847–858. <https://doi.org/10.1002/gbc.20074>
- Bushinsky, S. M., Gray, A. R., Johnson, K. S., & Sarmiento, J. L. (2017). Oxygen in the southern ocean from argo floats: Determination of processes driving air-sea fluxes. *Journal of Geophysical Research: Oceans*, 122, 8661–8682. <https://doi.org/10.1002/2017JC012923>
- Cael, B. B., & Follows, M. J. (2016). On the temperature dependence of oceanic export efficiency. *Geophysical Research Letters*, 43, 5170–5175. <https://doi.org/10.1002/2016GL068877>
- Campbell, J., Antoine, D., Armstrong, R., Arrigo, K., Balch, W., Barber, R., et al. (2002). Comparison of algorithms for estimating ocean primary production from surface chlorophyll, temperature, and irradiance. *Global Biogeochemical Cycles*, 16(3), 1035. <https://doi.org/10.1029/2001GB001444>
- Carr, M.-E. (2002). Estimation of potential productivity in eastern boundary currents using remote sensing. *Deep Sea Research Part II: Topical Studies in Oceanography*, 49(1), 59–80. [https://doi.org/10.1016/S0967-0645\(01\)00094-7](https://doi.org/10.1016/S0967-0645(01)00094-7)
- Carr, M., Friedrichs, M., Schmeltz, M., Noguchiatita, M., Antoine, D., Arrigo, K., et al. (2006). A comparison of global estimates of marine primary production from ocean color. *Deep Sea Research Part II: Topical Studies in Oceanography*, 53(5–7), 741–770. <https://doi.org/10.1016/j.dsr2.2006.01.028>
- Cavan, E. L., Henson, S. A., Belcher, A., & Sanders, R. (2017). Role of zooplankton in determining the efficiency of the biological carbon pump. *Biogeosciences*, 14(1), 177–186. <https://doi.org/10.5194/bg-14-177-2017>
- Cavan, E. L., Le Moigne, F. A. C., Poulton, A. J., Tarling, G. A., Ward, P., Daniels, C. J., et al. (2015). Attenuation of particulate organic carbon flux in the scotia sea, southern ocean, is controlled by zooplankton fecal pellets. *Geophysical Research Letters*, 42, 821–830. <https://doi.org/10.1002/2014GL062744>
- Churnside, J. H., & Thorne, R. E. (2005). Comparison of airborne lidar measurements with 420 khz echo-sounder measurements of zooplankton. *Applied Optics*, 44(26), 5504–5511. <https://doi.org/10.1364/AO.44.005504>
- Churnside, J. H., Wilson, J. J., & Tatarskii, V. V. (1997). Lidar profiles of fish schools. *Applied Optics*, 36(24), 6011–6020. <https://doi.org/10.1364/AO.36.006011>
- DeVries, T., & Weber, T. (2017). The export and fate of organic matter in the ocean: New constraints from combining satellite and oceanographic tracer observations. *Global Biogeochemical Cycles*, 31, 535–555. <https://doi.org/10.1002/2016GB005551>

- Dickey, T. D., Kattawar, G. W., & Voss, K. J. (2011). Shedding new light on light in the ocean. *Physics Today*, 64(4), 44–49. <https://doi.org/10.1063/1.3580492>
- Dong, S., Sprintall, J., Gille, S. T., & Talley, L. (2008). Southern ocean mixed-layer depth from argo float profiles. *Journal of Geophysical Research*, 113, C06013. <https://doi.org/10.1029/2006JC004051>
- Ducklow, H. W., & Doney, S. C. (2013). What is the metabolic state of the oligotrophic ocean? A debate. *Annual Review of Marine Science*, 5(1), 525–533. <https://doi.org/10.1146/annurev-marine-121211-172331>
- Dunne, J. P., Armstrong, R. A., Gnanadesikan, A., & Sarmiento, J. L. (2005). Empirical and mechanistic models for the particle export ratio. *Global Biogeochemical Cycles*, 19, GB4026. <https://doi.org/10.1029/2004GB002390>
- Dunne, J. P., Sarmiento, J. L., & Gnanadesikan, A. (2007). A synthesis of global particle export from the surface ocean and cycling through the ocean interior and on the seafloor. *Global Biogeochemical Cycles*, 21, GB4006. <https://doi.org/10.1029/2006GB002907>
- Emerson, S. (2014). Annual net community production and the biological carbon flux in the ocean. *Global Biogeochemical Cycles*, 28, 14–28. <https://doi.org/10.1002/2013GB004680>
- Eppley, R. W., & Peterson, B. J. (1979). Particulate organic matter flux and planktonic new production in the deep ocean. *Nature*, 282, 677–680.
- Friedrichs, M. A., Carr, M.-E., Barber, R. T., Scardi, M., Antoine, D., Armstrong, R. A., et al. (2009). Assessing the uncertainties of model estimates of primary productivity in the tropical pacific ocean. *Journal of Marine Systems*, 76, 113–133. <https://doi.org/10.1016/j.jmarsys.2008.05.010>
- Garcia, H. E., Locarnini, R. A., Boyer, T. P., Antonov, J. I., Baranova, O. K., Zweng, M. M., et al. (2014). *World Ocean Atlas 2013, Volume 4: Dissolved inorganic nutrients (phosphate, nitrate, silicate)*. In Levitus, S., & Mishonov, A. (Eds.), (NOAA Atlas NESDIS 76, 25 pp.). Retrieved from <https://www.nodc.noaa.gov/OC5/woa13/pubwoa13.html>
- Geider, R. J. (1987). Light and temperature dependence of the carbon to chlorophyll ratio in microalgae and cyanobacteria: Implications for physiology and growth of phytoplankton. *New Phytologist*, 106(1), 1–34. <https://doi.org/10.1111/j.1469-8137.1987.tb04788.x>
- Geider, R. J., & LaRoche, J. (1994). The role of iron in phytoplankton photosynthesis, and the potential for iron-limitation of primary productivity in the sea. *Photosynthesis Research*, 39, 275–301.
- Graff, J. R., Westberry, T. K., Milligan, A. J., Brown, M. B., Dall’Omo, G., van Dongen-Vogels, V., et al. (2015). Analytical phytoplankton carbon measurements spanning diverse ecosystems. *Deep Sea Research Part I: Oceanographic Research Papers*, 102, 16–25. <https://doi.org/10.1016/j.dsr.2015.04.006>
- Haëntjens, N., Boss, E., & Talley, L. D. (2017). Revisiting ocean color algorithms for chlorophyll a and particulate organic carbon in the southern ocean using biogeochemical floats. *Journal of Geophysical Research: Oceans*, 122, 6583–6593. <https://doi.org/10.1002/2017JC012844>
- Hennon, T. D., Riser, S. C., & Mecking, S. (2016). Profiling float-based observations of net respiration beneath the mixed layer. *Global Biogeochemical Cycles*, 30, 920–932. <https://doi.org/10.1002/2016GB005380>
- Henson, S. A., Sanders, R., Madsen, E., Morris, P. J., Le Moigne, F., & Quartly, G. D. (2011). A reduced estimate of the strength of the ocean’s biological carbon pump. *Geophysical Research Letters*, 38, L04606. <https://doi.org/10.1029/2011GL046735>
- Henson, S. A., Yool, A., & Sanders, R. (2015). Variability in efficiency of particulate organic carbon export: A model study. *Global Biogeochemical Cycles*, 29, 33–45. <https://doi.org/10.1002/2014GB004965>
- Hoge, F. E., Wright, C. W., Krabill, W. B., Buntzen, R. R., Gilbert, G. D., Swift, R. N., et al. (1988). Airborne lidar detection of subsurface oceanic scattering layers. *Applied Optics*, 27(19), 3969–3977. <https://doi.org/10.1364/AO.27.003969>
- Hunt, W. H., Winker, D. M., Vaughan, M. A., Powell, K. A., Lucker, P. L., & Weimer, C. (2009). Calipso lidar description and performance assessment. *Journal of Atmospheric and Oceanic Technology*, 26(7), 1214–1228. <https://doi.org/10.1175/2009JTECHA1223.1>
- Johnson, K. S., Plant, J. N., Dunne, J. P., Talley, L. D., & Sarmiento, J. L. (2017). Annual nitrate drawdown observed by soccom profiling floats and the relationship to annual net community production. *Journal of Geophysical Research: Oceans*, 122, 6668–6683. <https://doi.org/10.1002/2017JC012839>
- Laurenceau-Cornec, E. C., Trull, T. W., Davies, D. M., Bray, S. G., Doran, J., Planchon, F., et al. (2015). The relative importance of phytoplankton aggregates and zooplankton fecal pellets to carbon export: Insights from free-drifting sediment trap deployments in naturally iron-fertilised waters near the kerguelen plateau. *Biogeosciences*, 12(4), 1007–1027. <https://doi.org/10.5194/bg-12-1007-2015>
- Laws, E. A., D’sa, E., & Naik, P. (2011). Simple equations to estimate ratios of new or export production to total production from satellite-derived estimates of sea surface temperature and primary production. *Limnology and Oceanography: Methods*, 9(12), 593–601. <https://doi.org/10.4319/lom.2011.9.593>
- Laws, E. A., Falkowski, P. G., Smith, W. O., Ducklow, H., & McCarthy, J. J. (2000). Temperature effects on export production in the open ocean. *Global Biogeochemical Cycles*, 14(4), 1231–1246. <https://doi.org/10.1029/1999GB001229>
- Le Moigne, F. A. C., Henson, S. A., Cavan, E., Georges, C., Pabortsava, K., Achterberg, E. P., et al. (2016). What causes the inverse relationship between primary production and export efficiency in the southern ocean? *Geophysical Research Letters*, 43, 4457–4466. <https://doi.org/10.1002/2016GL068480>
- Lee, Z. P., Carder, K. L., Marra, J., Steward, R. G., & Perry, M. J. (1996). Estimating primary production at depth from remote sensing. *Applied Optics*, 35(3), 463–474. <https://doi.org/10.1364/AO.35.000463>
- Lourey, M. J., & Trull, T. W. (2001). Seasonal nutrient depletion and carbon export in the subantarctic and polar frontal zones of the southern ocean south of australia. *Journal of Geophysical Research*, 106(C12), 31463–31487. <https://doi.org/10.1029/2000JC000287>
- MacCreedy, P., & Quay, P. (2001). Biological export flux in the southern ocean estimated from a climatological nitrate budget. *Deep Sea Research Part II: Topical Studies in Oceanography*, 48(19), 4299–4322. [https://doi.org/10.1016/S0967-0645\(01\)00090-X](https://doi.org/10.1016/S0967-0645(01)00090-X)
- MacIntyre, H. L., Kana, T. M., & Geider, R. J. (2000). The effect of water motion on short-term rates of photosynthesis by marine phytoplankton. *Trends in Plant Science*, 5(1), 12–17. [https://doi.org/10.1016/S1360-1385\(99\)01504-6](https://doi.org/10.1016/S1360-1385(99)01504-6)
- Maiti, K., Charette, M. A., Buesseler, K. O., & Kahru, M. (2013). An inverse relationship between production and export efficiency in the southern ocean. *Geophysical Research Letters*, 40, 1557–1561. <https://doi.org/10.1002/grl.50219>
- Marra, J., & Ho, C., & Trees, C. C. (2003). *An algorithm for the calculation of primary productivity from remote sensing data* (Technical report number: LDEO-2003-1). Palisades, NY: Lamont-Doherty Earth Observatory.
- Martin, J. (1990). Glacial-interglacial CO<sub>2</sub> change: The iron hypothesis. *Paleoceanography*, 5(1), 1–13. <https://doi.org/10.1029/PA0051001p00001>
- Martz, T. R., Johnson, K. S., & Riser, S. C. (2008). Ocean metabolism observed with oxygen sensors on profiling floats in the south pacific. *Limnology and Oceanography: Methods*, 53(5 part 2), 2094–2111. [https://doi.org/10.4319/lo.2008.53.5\\_part\\_2.2094](https://doi.org/10.4319/lo.2008.53.5_part_2.2094)
- McNeil, B., & Tilbrook, B. (2009). A seasonal carbon budget for the sub-antarctic ocean, south of australia. *Marine Chemistry*, 115(3), 196–210. <https://doi.org/10.1016/j.marchem.2009.08.006>
- Moore, J. K., & Abbott, M. R. (2000). Phytoplankton chlorophyll distributions and primary production in the southern ocean. *Journal of Geophysical Research*, 105(C12), 28709–28722. <https://doi.org/10.1029/1999JC000043>

- Morel, A., Huot, Y., Gentili, B., Werdell, P. J., Hooker, S. B., & Franz, B. A. (2007). Examining the consistency of products derived from various ocean color sensors in open ocean (case 1) waters in the perspective of a multi-sensor approach. *Remote Sensing of Environment*, 111(1), 69–88. <https://doi.org/10.1016/j.rse.2007.03.012>
- Munro, D. R., Lovenduski, N. S., Stephens, B. B., Newberger, T., Arrigo, K. R., Takahashi, T., et al. (2015). Estimates of net community production in the southern ocean determined from time series observations (20022011) of nutrients, dissolved inorganic carbon, and surface ocean pCO<sub>2</sub> in drake passage. *Deep Sea Research Part II: Topical Studies in Oceanography*, 114(Suppl. C), 49–63. <https://doi.org/10.1016/j.dsr2.2014.12.014>
- Orsi, A. H., Whitworth, T., & Nowlin, W. D. (1995). On the meridional extent and fronts of the antarctic circumpolar current. *Deep Sea Research Part I: Oceanographic Research Papers*, 42(5), 641–673. [https://doi.org/10.1016/0967-0637\(95\)00021-W](https://doi.org/10.1016/0967-0637(95)00021-W)
- Packard, G. C., & Boardman, T. J. (1988). The misuse of ratios, indices, and percentages in ecophysiological research. *Physiological Zoology*, 61(1), 1–9.
- Pahlow, M., Dietze, H., & Oschlies, A. (2013). Optimality-based model of phytoplankton growth and diazotrophy. *Marine Ecology Progress Series*, 489, 1–16. <https://doi.org/10.3354/meps10449>
- Pearson, K. (1896). Mathematical contributions to the theory of evolution on a form of spurious correlation which may arise when indices are used in the measurement of organs. *Proceedings of the Royal Society of London*, 60, (359–367), 489–498. <https://doi.org/10.1098/rspl.1896.0076>
- Prairie, Y. T., & Bird, D. F. (1989). Some misconceptions about the spurious correlation problem in the ecological literature. *Oecologia*, 81(2), 285–288. <https://doi.org/10.1007/BF00379817>
- Riser, S. C., & Johnson, K. S. (2008). Net production of oxygen in the subtropical ocean. *Nature*, 451, 323–326. <https://doi.org/10.1038/nature06441>
- Roemmich, D., & Gilson, J. (2009). The 2004–2008 mean and annual cycle of temperature, salinity, and steric height in the global ocean from the argo program. *Progress in Oceanography*, 82(2), 81–100. <https://doi.org/10.1016/j.pocean.2009.03.004>
- Sanders, R., Morris, P. J., Poulton, A. J., Stinchcombe, M. C., Charalampopoulou, A., Lucas, M. I., & Thomalla, S. J. (2010). Does a ballast effect occur in the surface ocean? *Geophysical Research Letters*, 37, L08602. <https://doi.org/10.1029/2010GL042574>
- Sarmiento, J. L., & Bender, M. (1994). Carbon biogeochemistry and climate change. *Photosynthesis Research*, 39(3), 209–234. <https://doi.org/10.1007/BF00014585>
- Sarmiento, J. L., Gruber, N., Brzezinski, M. A., & Dunne, J. P. (2004a). High-latitude controls of thermocline nutrients and low latitude biological productivity. *Nature*, 427, 56–60. <https://doi.org/10.1038/nature02127>
- Sarmiento, J. L., & Orr, J. C. (1991). Three-dimensional simulations of the impact of southern ocean nutrient depletion on atmospheric CO<sub>2</sub> and ocean chemistry. *Limnology and Oceanography*, 36(8), 1928–1950. <https://doi.org/10.4319/lo.1991.36.8.1928>
- Sarmiento, J. L., Slater, R., Barber, R., Bopp, L., Doney, S. C., Hirst, A. C., et al. (2004b). Response of ocean ecosystems to climate warming. *Global Biogeochemical Cycles*, 18, GB3003. <https://doi.org/10.1029/2003GB002134>
- Schlitzer, R. (2002). Carbon export fluxes in the southern ocean: Results from inverse modeling and comparison with satellite-based estimates. *Deep Sea Research Part II: Topical Studies in Oceanography*, 49(9), 1623–1644. [https://doi.org/10.1016/S0967-0645\(02\)00004-8](https://doi.org/10.1016/S0967-0645(02)00004-8)
- Shadwick, E. H., Trull, T. W., Tilbrook, B., Sutton, A. J., Schulz, E., & Sabine, C. L. (2015). Seasonality of biological and physical controls on surface ocean CO<sub>2</sub> from hourly observations at the southern ocean time series site south of Australia. *Global Biogeochemical Cycles*, 29, 223–238. <https://doi.org/10.1002/2014GB004906>
- Shang, S. L., Behrenfeld, M. J., Lee, Z. P., O'Malley, R. T., Wei, G. M., et al. (2010). Comparison of primary production models in the Southern Ocean—Preliminary results. In Hou, W., & Arnone, R. (Eds.), *Proceeding SPIE 7678, Ocean Sensing and Monitoring II*. <https://doi.org/10.1117/12.853631>
- Siegel, D. A., Buesseler, K. O., Doney, S. C., Salliey, S. F., Behrenfeld, M. J., & Boyd, P. W. (2014). Global assessment of ocean carbon export by combining satellite observations and food-web models. *Global Biogeochemical Cycles*, 28, 181–196. <https://doi.org/10.1002/2013GB004743>
- Sunda, W. G., & Huntsman, S. A. (1997). Interrelated influence of iron, light and cell size on marine phytoplankton growth. *Nature*, 390, 389–392. <https://doi.org/10.1038/37093>
- Thomalla, S. J., Ogunkoya, A. G., Vichi, M., & Swart, S. (2017). Using optical sensors on gliders to estimate phytoplankton carbon concentrations and chlorophyll-to-carbon ratios in the southern ocean. *Frontiers in Marine Science*, 4, 34. <https://doi.org/10.3389/fmars.2017.00034>
- Volk, T., & Hoffert, M. (1985). Ocean carbon pumps: Analysis of relative strengths and efficiencies in ocean-driven atmospheric CO<sub>2</sub> changes. In E. Sundquist and W. Broecker (Eds.), *The carbon cycle and atmospheric CO<sub>2</sub>: Natural variations Archean to present. Chapman conference papers, 1984* ( Geophysical Monograph 32, pp. 99–110). Washington, DC: American Geophysical Union.
- Westberry, T., Behrenfeld, M. J., Siegel, D. A., & Boss, E. (2008). Carbon-based primary productivity modeling with vertically resolved photoacclimation. *Global Biogeochemical Cycles*, 22, GB2024. <https://doi.org/10.1029/2007GB003078>
- Winker, D. M., Vaughan, M. A., Omar, A., Hu, Y., Powell, K. A., Liu, Z., et al. (2009). Overview of the CALIPSO mission and CALIOP data processing algorithms. *Journal of Atmospheric and Oceanic Technology*, 26(11), 2310–2323. <https://doi.org/10.1175/2009JTECHA1281.1>
- York, D. (1966). Least-squares fitting of a straight line. *Canadian Journal of Physics*, 44(5), 1079–1086. <https://doi.org/10.1139/p66-090>